Experimental Study of J/ψ Radiative Decay to $\pi^+\pi^-$

BES Collaboration

T.N.Ruan[a], D.V.Bugg[b]

a. Department of Modern Physics, University of Science and Technology of China, Hefei, Anhui 230026, P.R.China
b. Queen Mary and Westfield College, London E1 4NS, United Kingdom
c. IHEP, Beijing, P.R.China

Abstract

The BES data on $J/\psi \to \gamma\pi^+\pi^-$ is presented. A new feature of the $\pi^+\pi^-$ data is the presence of $f_0(980)$ and $f_0(1500)$ which are required by two dips in the mass distribution, due to destructive interference with the broad 0^{++} resonance. In the mass region 1650-1800Mev, according to mass scan results, both 0^{++} and 2^{++} are needed in the fitting. A narrow 2^{++} resonance is also needed in fitting at higher mass region and its presence can be clearly seen in the mass and width's scan around 2.2 Gev. Some results are consistent with the corresponding results in the $J/\psi \to \gamma K^+K^-$ channel.

Introduction

There have been many earlier studies of J/ψ radiative decays to $\pi\pi$ and KK by Mark II [1], Mark III [2,3]and DM2 [4,5]. An important issue, reviewed recently by the Particle Data Group (PDG) [6], is the spin of $f_J(1710)$. Early data favored spin 2, and this appeared to be confirmed by the earliest results from the Omega collaboration on Central Production [7]. However, a recent re-analysis of Mark III data by Dunwoodie [8]has reversed earlier Mark III conclusion by favoring spin 0. Most recently, a fresh analysis of Central Production data by the WA102 group has also reversed the conclusion of the

Omega collaboration in favor of spin 0. Meanwhile, early BES results [10]favored a spin 2 resonance at 1696 Mev, but required in addition a spin 0 component at 1781 Mev. The existence of this $f_0(1770)$ component was also demonstrated in J/ψ radiative decays to 4π [11]. The $f_0(1770) \longrightarrow \eta\eta$ has been confirmed in Crystal Barrel data on $\bar{p}p \rightarrow (\eta\eta)\pi^0$ [12].

Previous analysis of J/ψ radiative decays to $\pi^+\pi^-$ has ignored the contribution from $f_0(1500)$, but we find it to play a significant role. Earlier analysis of $J/\psi \rightarrow \gamma(4\pi)$ [11]requires a component with branch ratio $BR[J/\psi \rightarrow \gamma f_0(1500), f_0(1500) \rightarrow 4\pi] = 2.1 \times 10^{-4}$. Using the result of Abele et al. [13] $BR[f_0(1500) \rightarrow \pi\pi]/BR[f_0(1500) \rightarrow 4\pi] = 0.83$, this requires $BR[J/\psi \rightarrow \gamma f_0(1500), f_0(1500) \rightarrow 2\pi] = 1.7 \times 10^{-4}$. But in the $\pi^+\pi^-$ invariant mass spectrum, there is a dip around 1.5 Gev. In $\pi\pi \rightarrow \pi\pi$, the dip is well known from amplitude analysis of CERN-Munich data [14]. It arises from destructive interference between $f_0(1500)$ and the very broad 0^{++} resonance. For the sake of convinience, we call this broad 0^{++} resonance as $f_0(1030)$ in this memo. Hence this broad component is required in fitting present data. After considering the interference between $f_0(1500)$ and the broad $f_0(1030)$, $f_0(1500)$ appears in the mass and width scan.

A similar case occurs in the $0.98Gev$ mass region. In the $\pi\pi$ mass spectrum, a dip appears here. It is commonly believed that $f_0(980)$ is not produced in radiative decays. But it is well known that $f_0(980)$ is not an ordinary $q\bar{q}$ meson state. After considering interferences between different 0^{++} resonances, we use a 0^{++} to scan this region and find a clear signal of a narrow 0^{++} resonance. The mass and width scan results are quite close to those of PDG values. Its branch ratio in this channel is relatively very large. That means that it is abundantly produced in J/ψ radiative decay. According to previously study[22], the $f_0(980)$ possesses couplings of the about the same strength to both s quark and u, d quarks[23]. All these strongly support that $f_0(980)$ is a 0^{++} glueball candidate or at least contains a lot of scalar glueball component.

A very narrow $f_2'(2230)$ has been studied in J/ψ radiative decay by BES previously [15,16]. The mass region around $2.2Gev$ is also studied in this work and some evidence is found for a narrow 2^{++} resonance in mass and width scan.

Event Selection

1. Initial Event Selection

   (a) Charged Track Selection Criteria

   - Two charged tracks with zero net charge, $N_{chrg} = 2$, $\sum Q = 0$.
   - Good helix fit for MDC tracks, MFIT = 2 or -19.
   - Polar angle of each track in MDC $|cos\theta| < 0.8$.
   - Event vertex: $\mid \sqrt{x_0^2 + y_0^2} \mid \leq 2\ cm$; $\mid z_0 \mid \leq 20cm$.
   - Transverse momentum $P_{xy} > 60Mev/c$.
   - Angle between two charged tracks is less than 175°.
   - Neither charged track is registered in the muon counters; this reduces $\gamma\mu\mu$ events.
   - Neither charged track deposits more than 0.6 Gev of energy in the shower counters; this suppresses radiative Bhabha events.

   (b) Photon Selection Criteria

   - Hit in BSC and $Layers > 1$.
   - $E_\gamma > 70$ MeV.
   - Shower starts before layer 6.
   - The number of shower counter paired hits should be larger than 3.
   - Angle between the cluster entering and going through BSC should be less than 30°.
   - Angle between neutral tracks and charged tracks should be larger than 10°.
   - At least one good photon.

   (c) Kinematical fit. All surviving events are submitted to the following $4C$ kinematic fits, $\gamma\pi^+\pi^-$ $\gamma\gamma\pi^+\pi^-$, γK^+K^-, and $\gamma\bar{p}p$, and in the initial data selection, it is required that $\chi^2(J/\psi \to \gamma\pi^+\pi^-) \leq 50$.

   We made no effort on π K identification in the initial data selection; all π K identification will be made in the final data selection. After initial data selection, the $\pi^+\pi^-$ invariant mass spectrum is shown in Fig. 1.

2. Final Event Selection

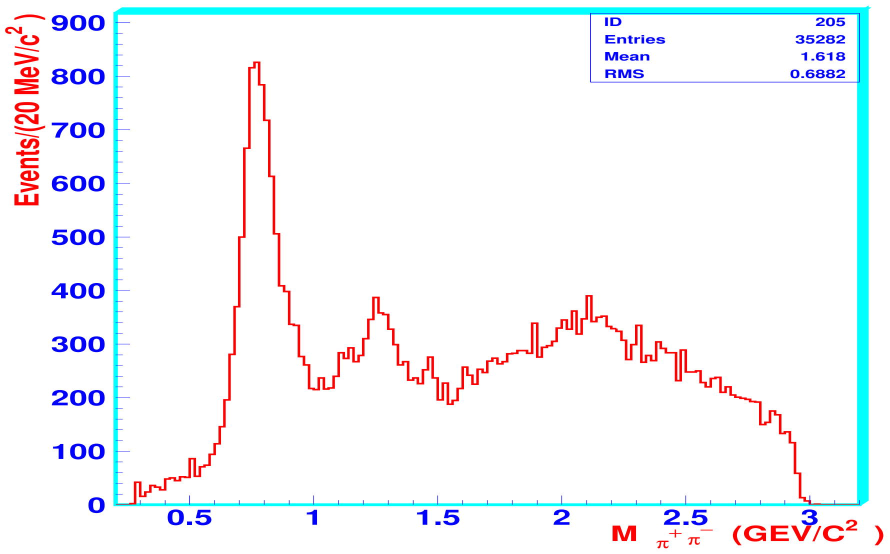

Figure 1: The $\pi^+\pi^-$ invariant masses spectrum (after initial event selection)

(a) $\chi^2(J/\psi \to \gamma\pi^+\pi^-)$ of $4C$ kinematic fits is less than or equal to 12.0.

(b) Momentums of two pions are denoted as $\vec{p}_1$ and $\vec{p}_2$ respectively. The $\vec{P}_{miss}$ is defined by the following relation:

$$\vec{P}_{miss} = -\vec{p}_1 - \vec{p}_2 \quad , \quad P_{miss} = |\vec{P}_{miss}|.$$

If two charged particles are supposed to be pions, then the energy of two pions can be calculated and E_{miss} is defined by:

$$E_{miss} = E_{J/\psi} - E_{\pi^+} - E_{\pi^-}.$$

Because the direction of photon is known, we can calculate the angle between the direction of the photon and the direction of $\vec{P}_{miss}$ and denote the corresponding value as α_1. If an event contains more than one photon, we can calculate all angles between all photons and $\vec{P}_{miss}$, and select the smallest one as α_1. The Monte Carlo distribution of sinα_1 in $J/\psi \to \gamma\pi^+\pi^-$ is shown in Fig.2. It is required that

$$\sin\alpha_1 \leq 0.15 \qquad or \qquad \alpha_1 \leq 8.6^\circ.$$

This cut condition helps us to remove some multi-photon events. But the main purpose of this cut condition is to improve the quality of data which is important to analyze $\rho\pi$ events.

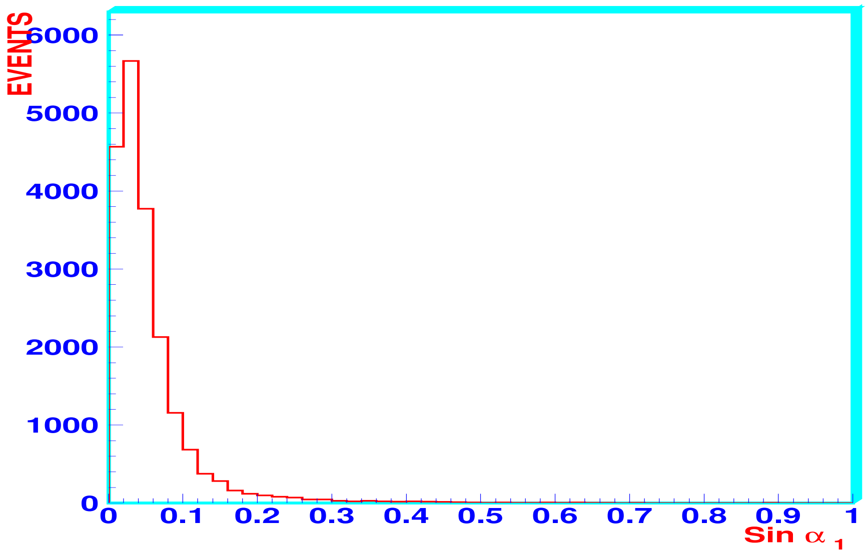

Figure 2: The sinα_1 distribution of $J/\psi \to \gamma\pi^+\pi^-$ Monte Carlo events

(c) Background events come form $J/\psi \to \pi^0\pi^+\pi^-$; Fig.4 shows that almost 50% of these events have more than one good photon. Fig.3 is the number of good photons in the $J/\psi \to \gamma\pi^+\pi^-$ Monte Carlo simulation and Fig.4 is the number of good photons in the $J/\psi \to \pi^0\pi^+\pi^-$ Monte Carlo simulation. So, in order to reduce background events coming from $J/\psi \to \pi^0\pi^+\pi^-$, $J/\psi \to \rho\pi$ and other decay process which contain more than one photon in the final states, it is required that the number of good photons = 1.

(d) In order to reduce background events from $J/\psi \to \gamma K^+K^-$, before we do the π K identification, we use information of $4C$ kinematic fits. All events have been submitted to $\gamma\pi^+\pi^-$ and γK^+K^- $4C$ kinematic fits in the initial data selection. Fig.5 and Fig.6 show the distributions of $\chi^2_{4C}(\gamma\pi\pi) - \chi^2_{4C}(\gamma KK) + 10.0$ of $J/\psi \to \gamma\pi^+\pi^-$ Monte Carlo events and $J/\psi \to \gamma K^+K^-$ Monte Carlo events respectively. From these two figures, it is easy to see that $\chi^2_{4C}(\gamma\pi^+\pi^-) \leq \chi^2_{4C}(\gamma K^+K^-) - 10.0$ is a suitable cut condition to reduce γK^+K^-

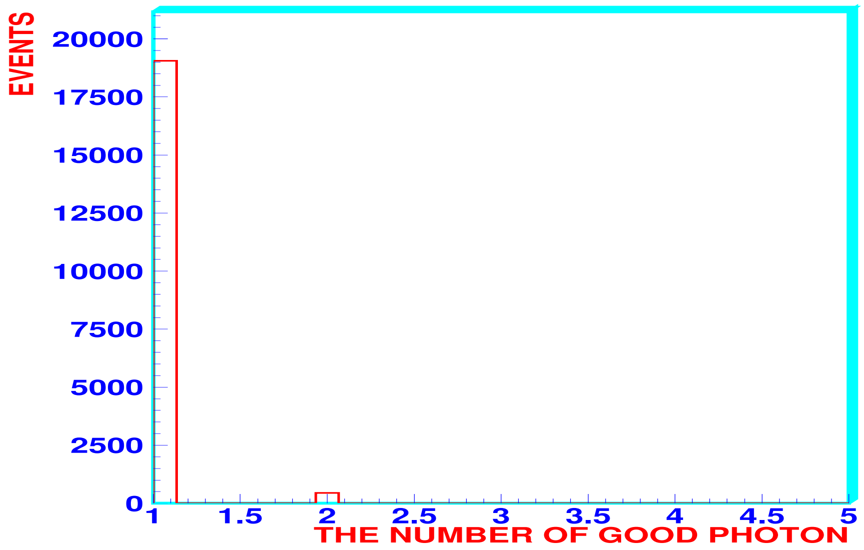

Figure 3: The distribution of the number of good photon in $J/\psi \to \gamma\pi^+\pi^-$ Monte Carlo events

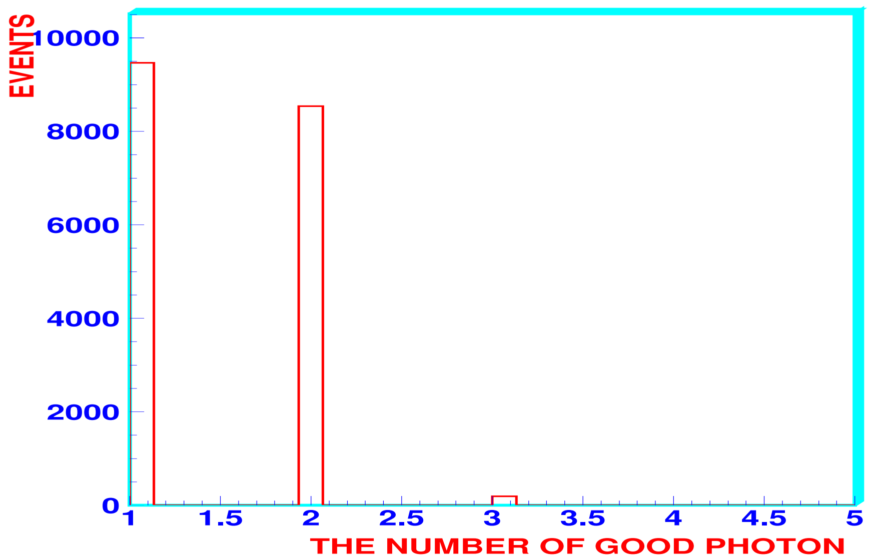

Figure 4: The distribution of the number of good photon in $J/\psi \to \pi^0\pi^+\pi^-$ Monte Carlo events

background events.

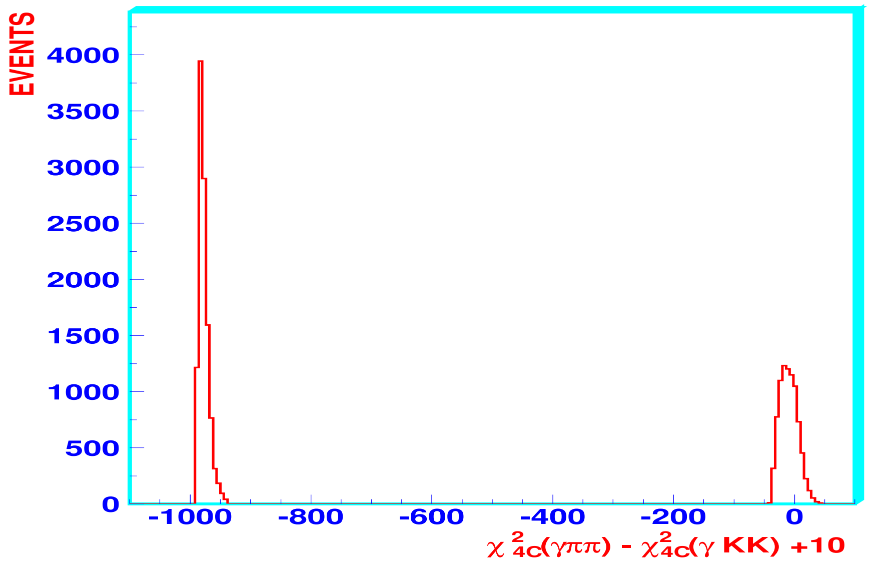

Figure 5: Distribution of $\chi^2_{4C}(\gamma\pi^+\pi^-) - \chi^2_{4C}(\gamma K^+K^-) + 10.0$ of $J/\psi \to \gamma\pi^+\pi^-$ Monte Carlo events

(e) TOF and some other information are used to identify π and K. TOF weights of charged particles can be directly read from the reconstructed BES data. For the charged particle i, its TOF weights for π and K are denoted as $WTPI(i)$ and $WTK(i)$ respectively. In the above discussion, we have defined P_{miss} and E_{miss}; the U_{miss} is defined as follows:

$$U_{miss} = E_{miss} - P_{miss}.$$

If we supposed that the charged particles are pions, Ks or protons, the corresponding U_{miss} is denoted as $U_{miss}(\pi)$, $U_{miss}(K)$ or $U_{miss}(p)$ respectively. Define:

$$WT = (WTPI(1) + WTPI(2) - WTK(1) - WTK(2))$$

$$- 6.0 \times U_{miss}(\pi) - 7.0 \times U_{miss}(K) - 5.0 \times U_{miss}(p) + M_{\pi\pi}.$$

In order to explain why we add $M_{\pi\pi}$ into the difinition of WT, let's first see the scatter plot of $WT - M\pi\pi$ for both $J/\psi \to \gamma\pi\pi$ and

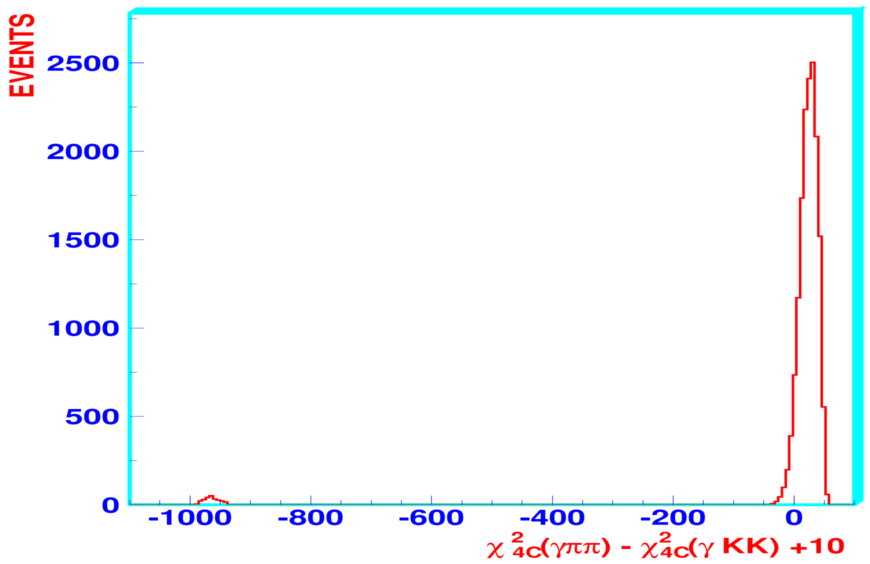

Figure 6: Distribution of $\chi^2_{4C}(\gamma\pi^+\pi^-) - \chi^2_{4C}(\gamma K^+K^-) + 10.0$ of $J/\psi \rightarrow \gamma K^+K^-$ Monte Carlo events

$J/\psi \rightarrow \gamma KK$ which is shown in Fig.7. In Fig.7, the left plot is for $J/\psi \rightarrow \gamma\pi\pi$ Monte Carlo events and the right plot is for $J/\psi \rightarrow \gamma KK$ Monte Carlo events. It could be seen that the scatter plot for $J/\psi \rightarrow \gamma\pi\pi$ Monte Carlo events is a little slope down with mass spectrum. If we require that $WT - M_{\pi\pi}$ is greater than a fixed value, then more events will be cut in the higher mass region. In order to make the the scatter plot for $J/\psi \rightarrow \gamma\pi\pi$ Monte Carlo events more flat with mass spectrum, we add $M_{\pi\pi}$ into WT. The scatter plot for WT is shown in Fig.8. Fig.9 and Fig.10 show the distribution of WT of $J/\psi \rightarrow \gamma\pi^+\pi^-$ and $J/\psi \rightarrow \gamma K^+K^-$ Monte Carlo events respectively. From these figures, we select a cut condition to identify pions:

$$WT \geq 5.0 \ .$$

(f) If we difine

$$WTOF = WTPI(1) + WTPI(2) - WTK(1) - WTK(2),$$

form the scatter plot in Fig.11, we can see that

$$WTOF \geq -0.6 \ .$$

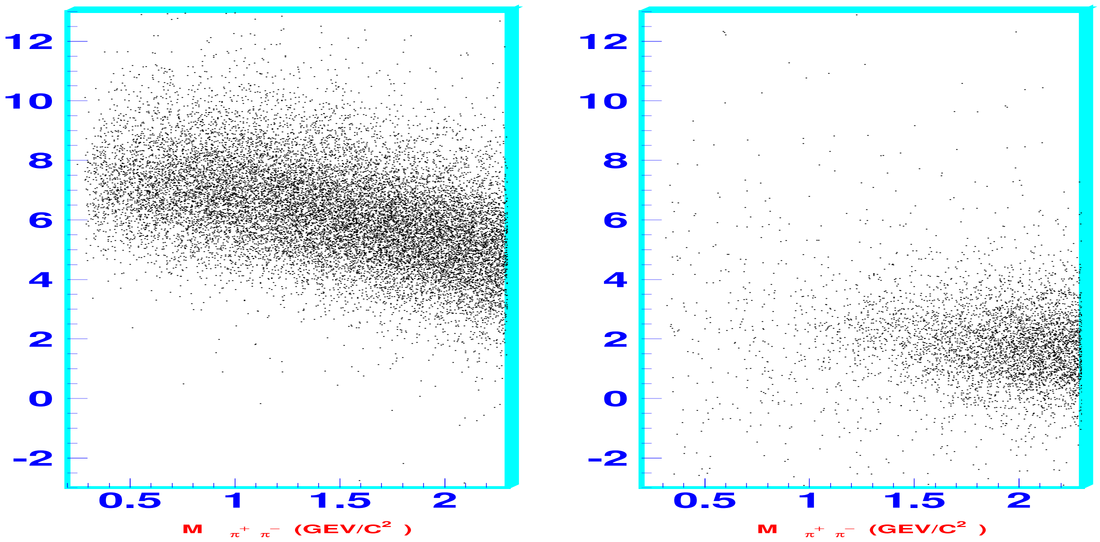

Figure 7: Distribution of $WT - M\pi\pi$ of $J/\psi \to \gamma\pi^+\pi^-$ (left) and $J/\psi \to \gamma K^+K^-$ (right) Monte Carlo events

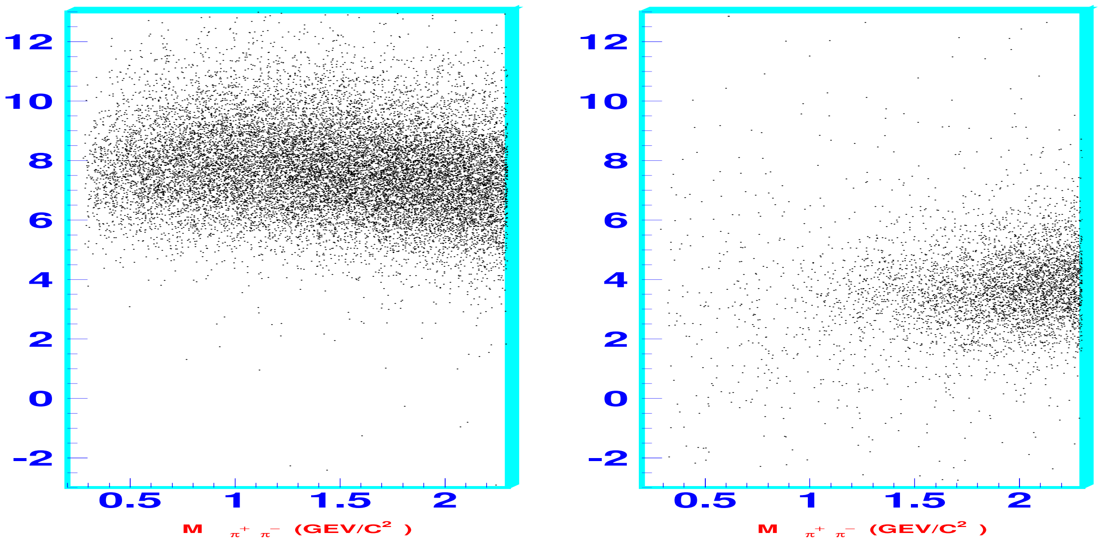

Figure 8: Distribution of WT of $J/\psi \to \gamma\pi^+\pi^-$ (left) and $J/\psi \to \gamma K^+K^-$ (right) Monte Carlo events

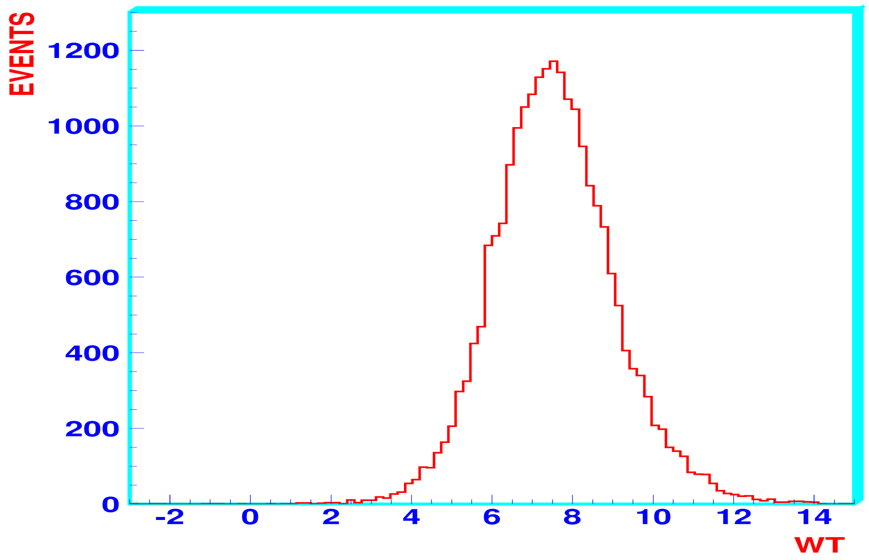

Figure 9: Distribution of WT of $J/\psi \to \gamma\pi^+\pi^-$ Monte Carlo events

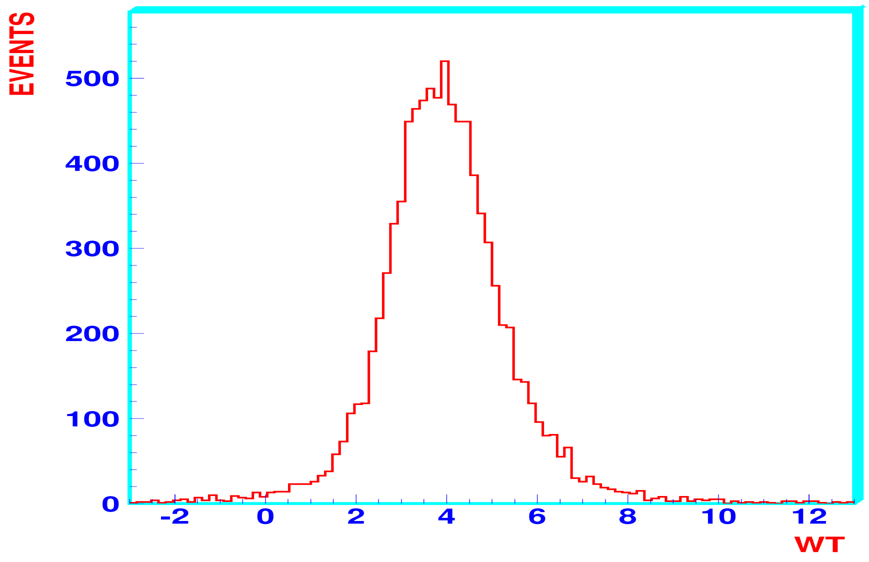

Figure 10: Distribution of WT of $J/\psi \to \gamma K^+K^-$ Monte Carlo events

can also remove some $J/\psi \to \gamma K^+K^-$ events.

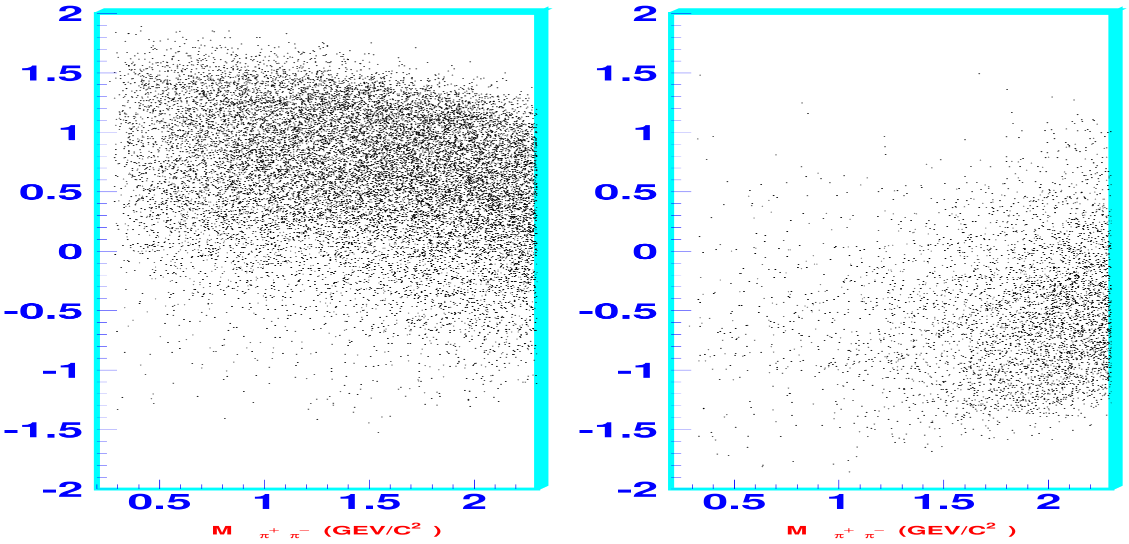

Figure 11: Distribution of $WTOF$ of $J/\psi \to \gamma\pi^+\pi^-$ (left) and $J/\psi \to \gamma K^+K^-$ (right) Monte Carlo events

(g) If the momentum of a charged particle is less than 0.6 Gev, the π/k identification given by TOF is reliable. This could be seen from scatter plot of Monte Carlo data (Fig.12) and BES data (Fig.13). So, we require that, if the momentum of the charged particle is less than 0.6 Gev, it should be identified as π by TOF.

(h) Finally, because our main interest is mainly concentrated on the middle mass region and the statistics above $2.3Gev$ is not high enough to perform a good analysis, we cut off all events above $2.3Gev$ by using the following cut condition:

$$M_{\pi\pi} \leq 2.3Gev.$$

Effects of various cut conditions are shown in table 1 and table 2. In table 1, the effect of single cut condition is shown while table 2 shows the effects of combined cut conditions. The $\pi^+\pi^-$ invariant mass spectrum after final event selection is shown in Fig.14 and the Dalitz plot is shown in Fig.15. The angular distribution of BES data in various mass region is shown in Fig.16–21 From

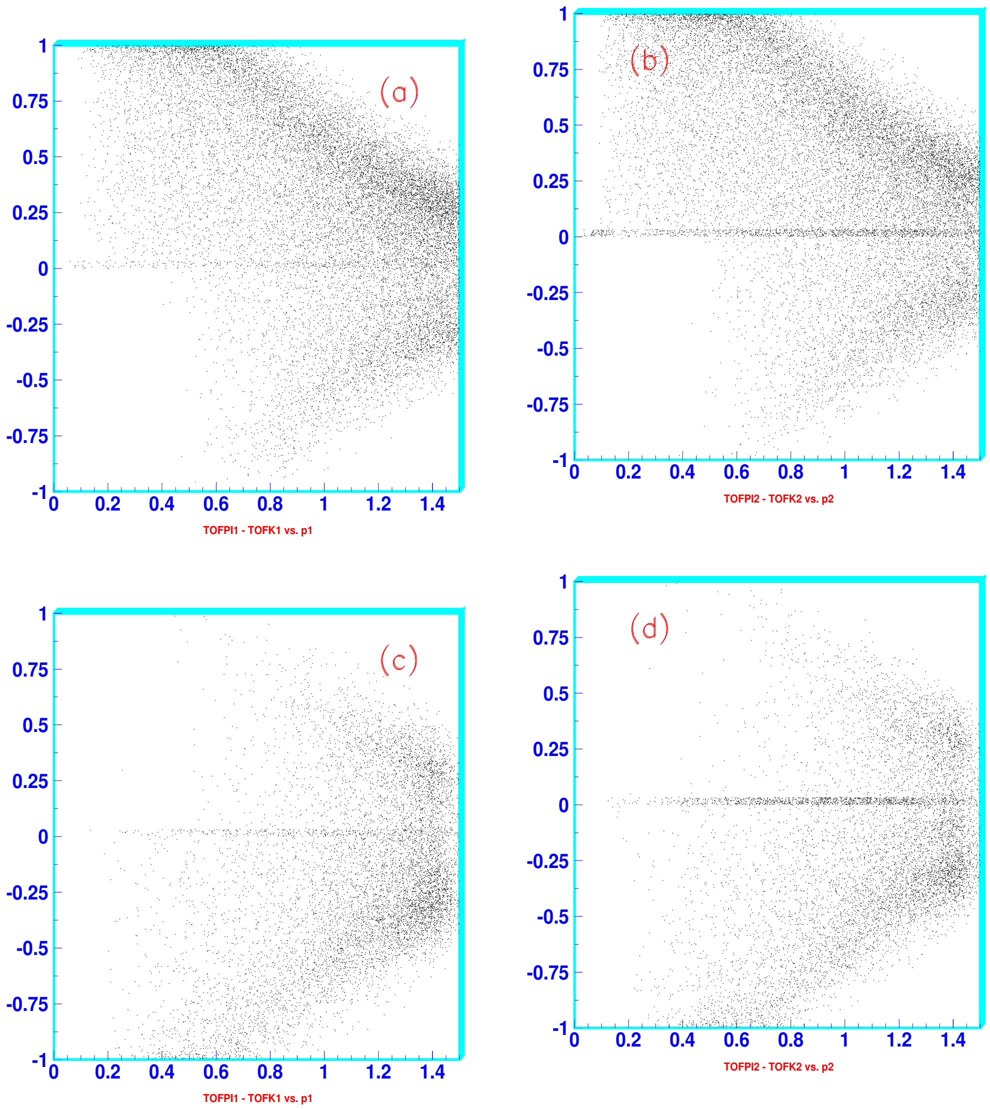

Figure 12: Scatter plots for relative TOF weight of $J/\psi \to \gamma\pi^+\pi^-$ Monte Carlo events ((a) and (b)) and $J/\psi \to \gamma K^+K^-$ Monte Carlo events ((c) and (d)).

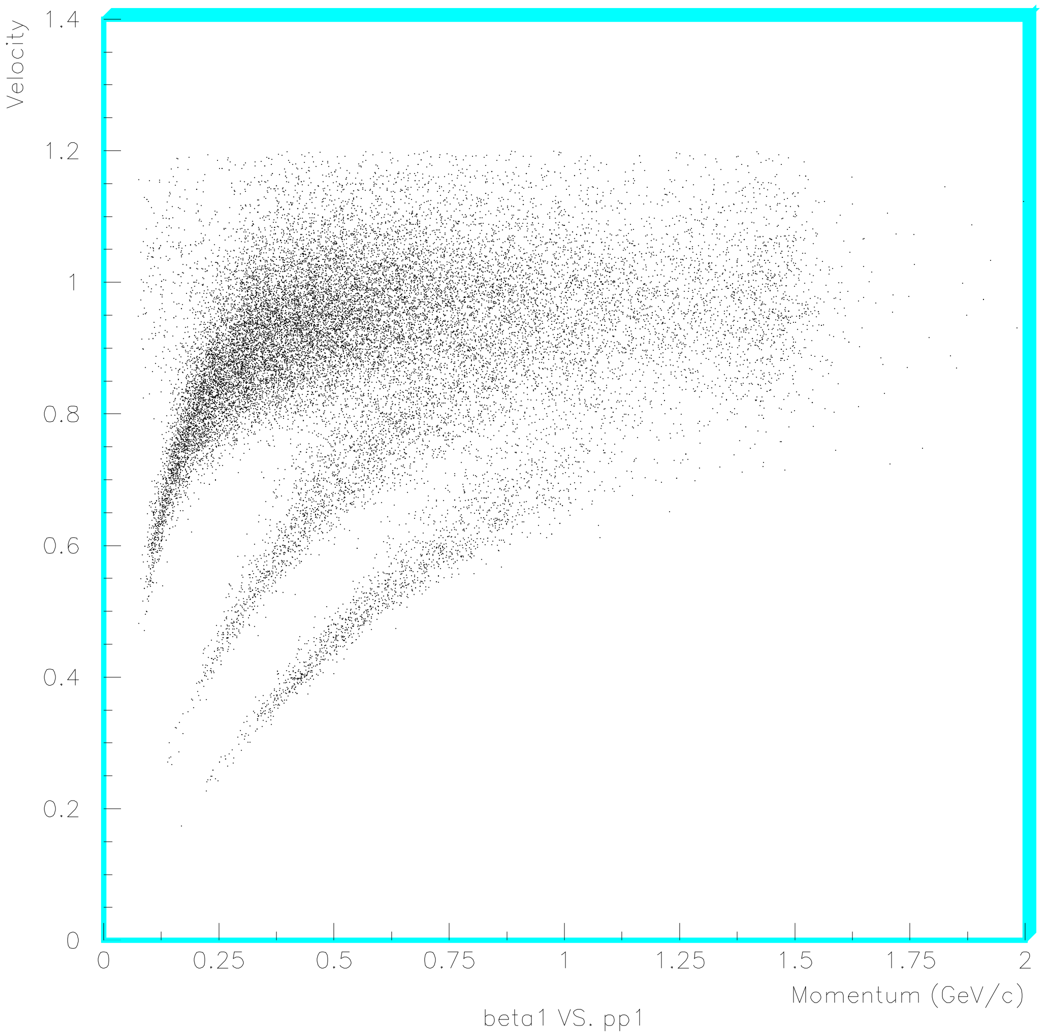

Figure 13: Scatter plot for the relativistic veloticities VS the momenta of the particles of BESI data.

cut	$\gamma\pi\pi$	γKK	$\rho\pi$	$\pi^0\pi\pi$
total events	50000	100000	100000	70000
initial cut	22538	9196	18048	16644
$\chi_{\gamma\pi\pi} < 12.$	13717	1127	6814	6156
$\chi_{\gamma\pi\pi} < \chi_{\gamma KK} - 10.$	21086	929	16243	15251
sin$\alpha_1 < 0.15$	21677	8205	17067	15654
good $\gamma = 1$	22096	8505	12835	11302
WTOF $>$ -0.6	21904	5922	17631	16182
WT $>$ 5.0	21690	1766	17309	15974
TOF Cut	22438	8240	17938	16561

Table 1: Effects of single cut conditions.

cut	$\gamma\pi\pi$	γKK	$\rho\pi$	$\pi^0\pi\pi$
total events	50000	100000	100000	70000
initial cut	22538	9196	18048	16644
$\chi_{\gamma\pi\pi} < 12.$	13717	1127	6814	6156
$\chi_{\gamma\pi\pi} < \chi_{\gamma KK} - 10.$	13268	446	6568	6008
TOF Cut	13209	403	6521	5980
WT $>$ 5.0	13092	326	6475	5943
WTOF $>$ -0.6	12799	260	6371	5821
good $\gamma = 1$	12591	242	5182	4653
sin$\alpha_1 < 0.15$	12369	228	5127	4611
$M_{\pi\pi} < 2.3$	10245	89	4515	4055

Table 2: Effects of combined cut conditions.

the Dalitz plot, we can clearly see $f_2(1270)$, $f_J(1710)$ and $\rho\pi$. Because $\rho^{\pm}\pi^{\mp}$ background is not cut off, the resonances around $2.0Gev$ or $2.2Gev$ region in the invariant mass spectrum is not very clear. But this does not affect our final analysis, for the angular distribution as well as the invariant mass distribution is considered in our analysis.

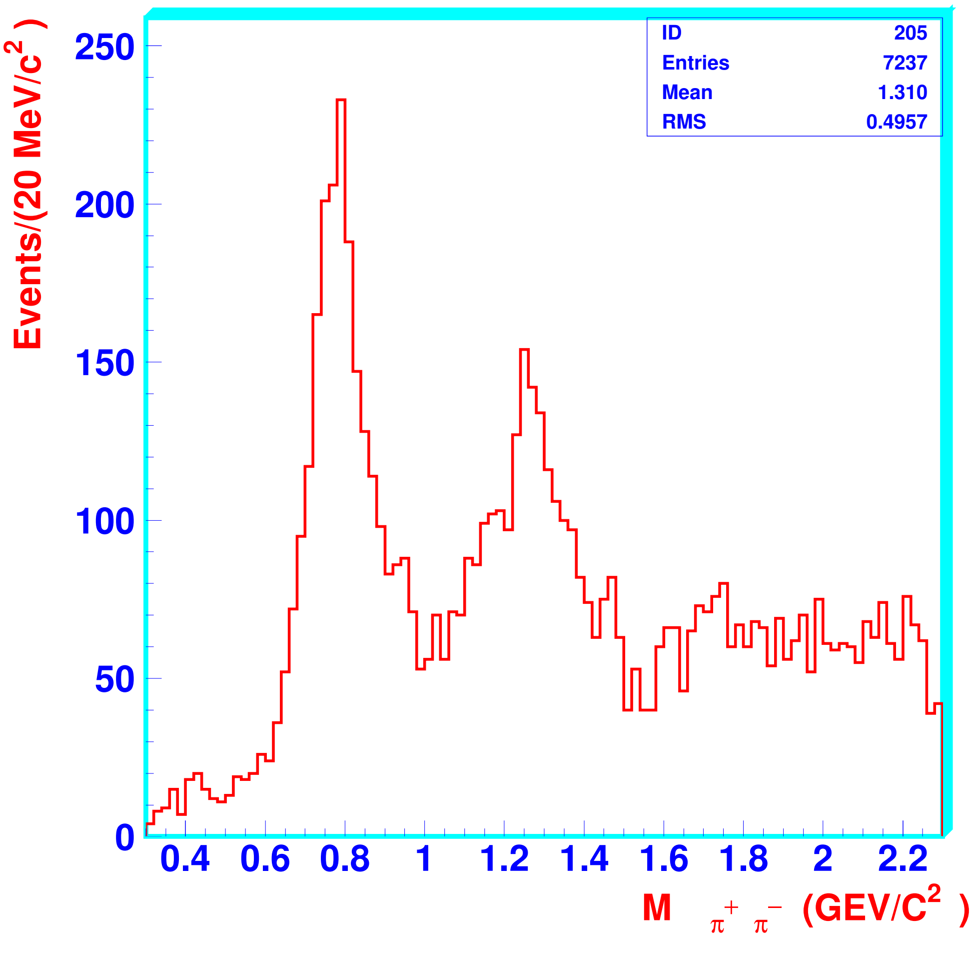

Figure 14: Invariant mass spectrum of $\pi^+\pi^-$ in $J/\psi \to \gamma\pi^+\pi^-$ (after final event selection)

In the event selection of $J/\psi \to \gamma\pi^+\pi^-$, the main background comes from

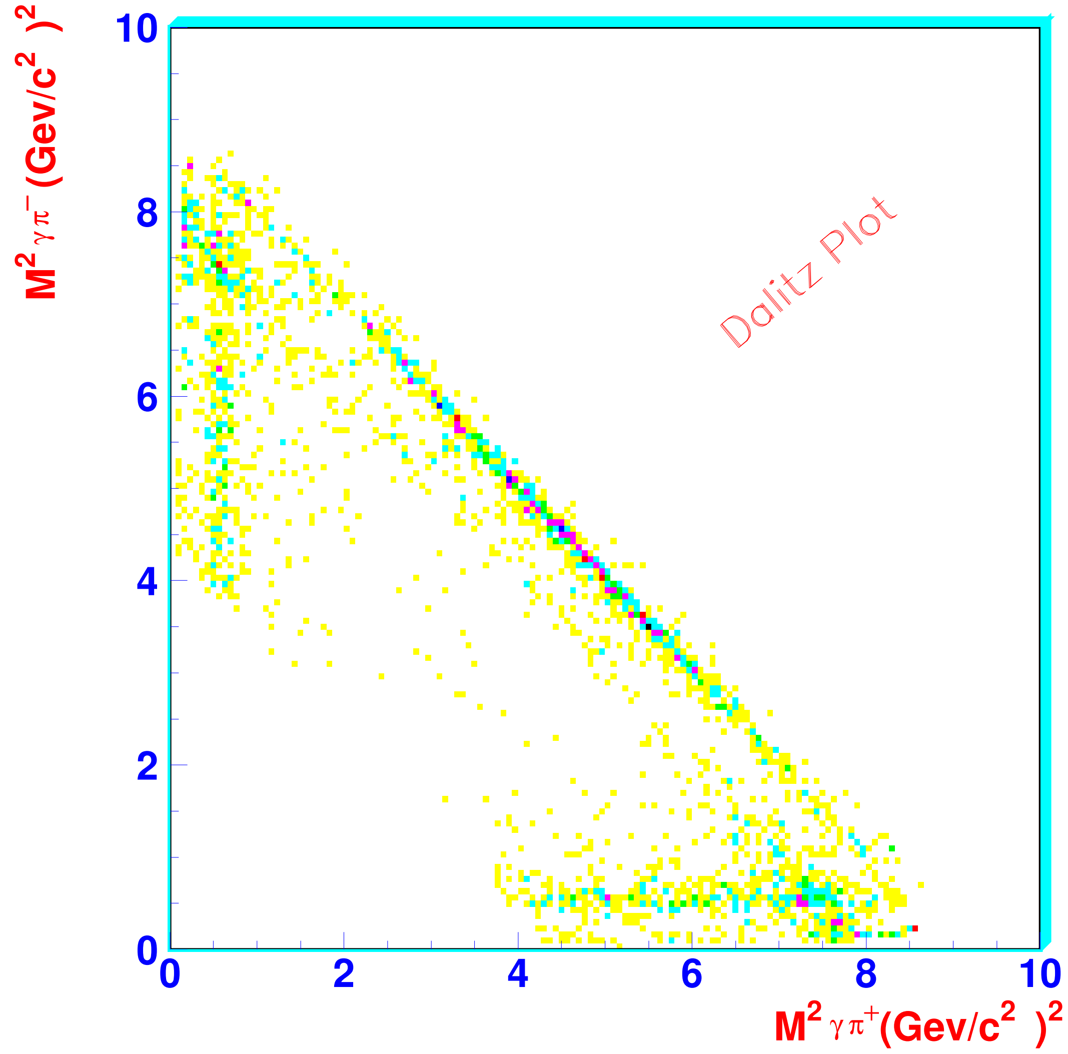

Figure 15: Dalitz plot (after final event selection)

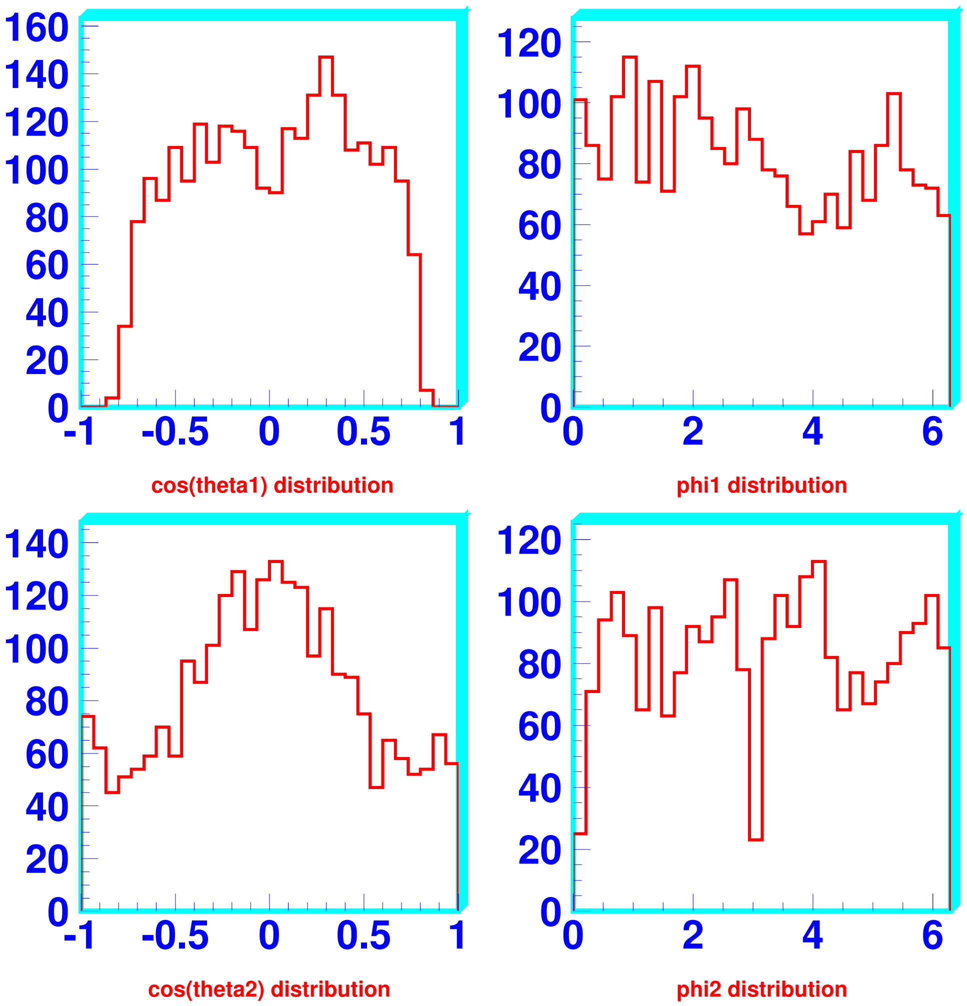

Figure 16: Angular distribution of BES data between 0.0 Gev — 1.0 Gev.

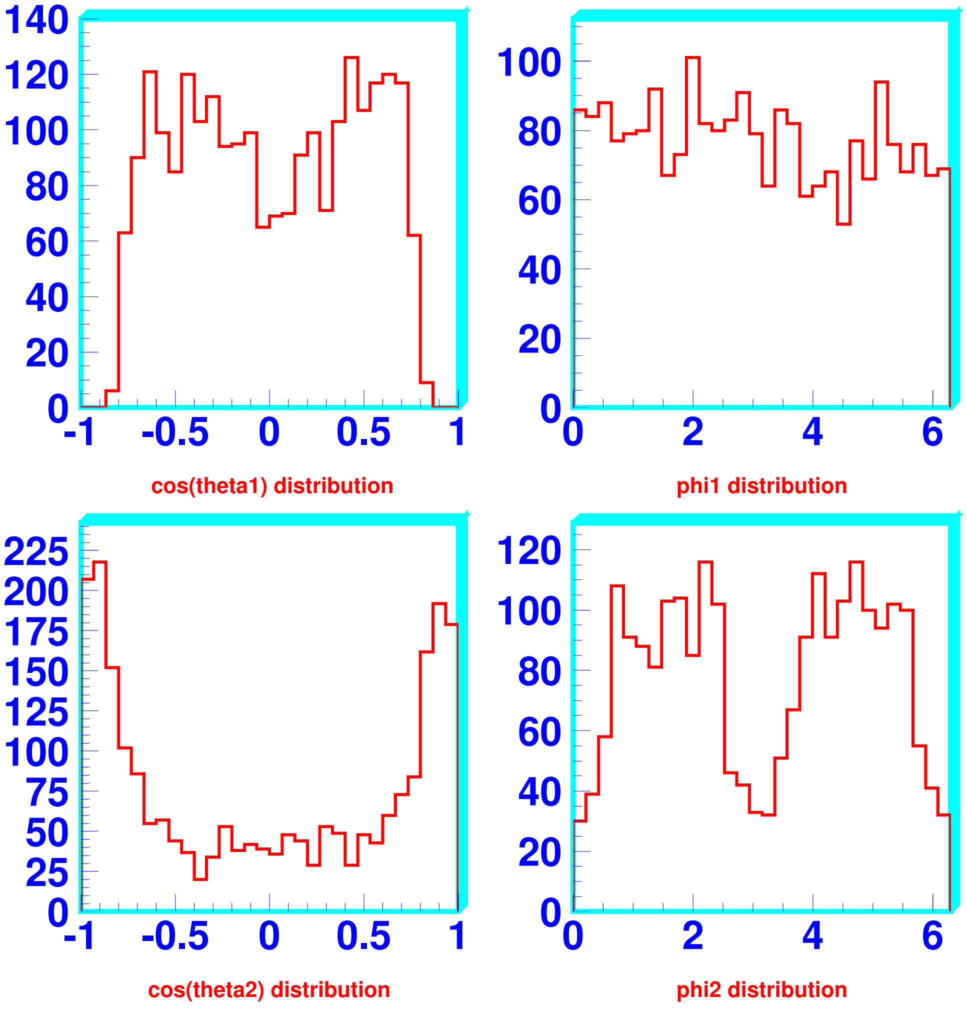

Figure 17: Angular distribution of BES data between 1.0 Gev — 1.5 Gev.

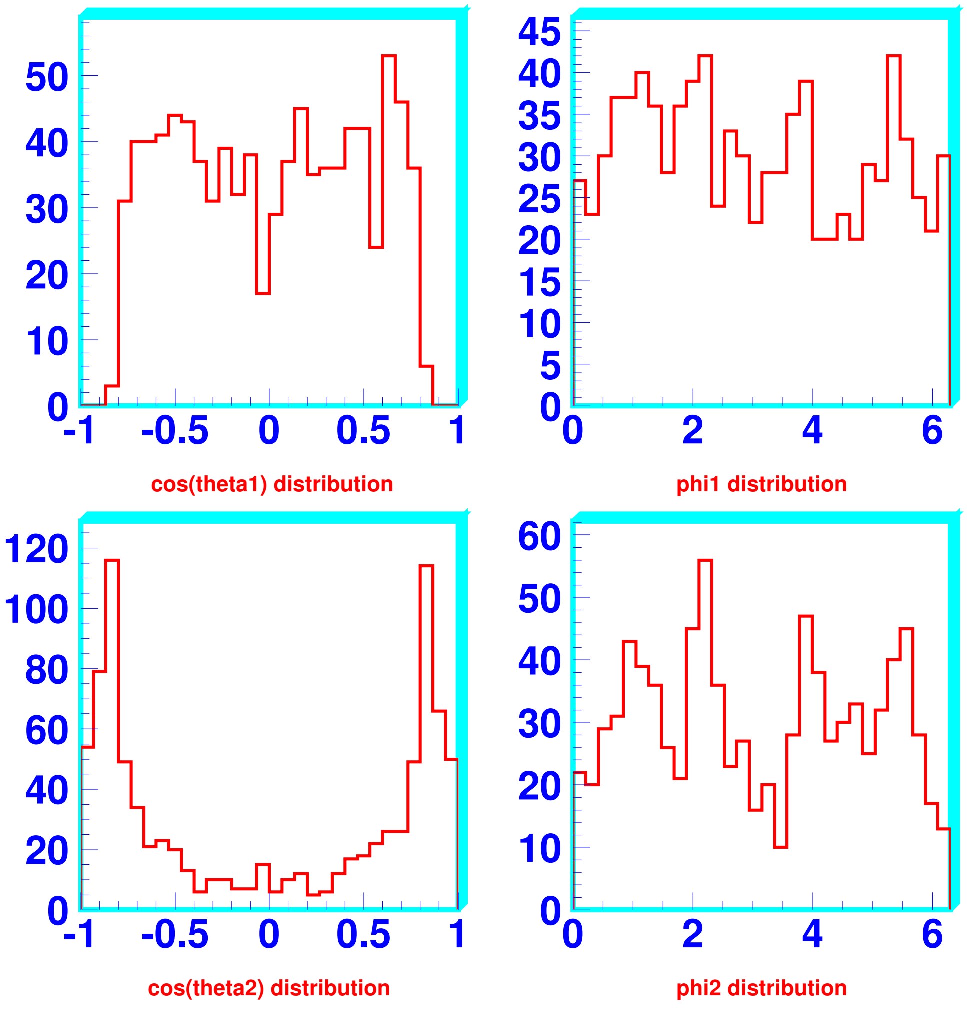

Figure 18: Angular distribution of BES data between 1.5 Gev — 1.8 Gev.

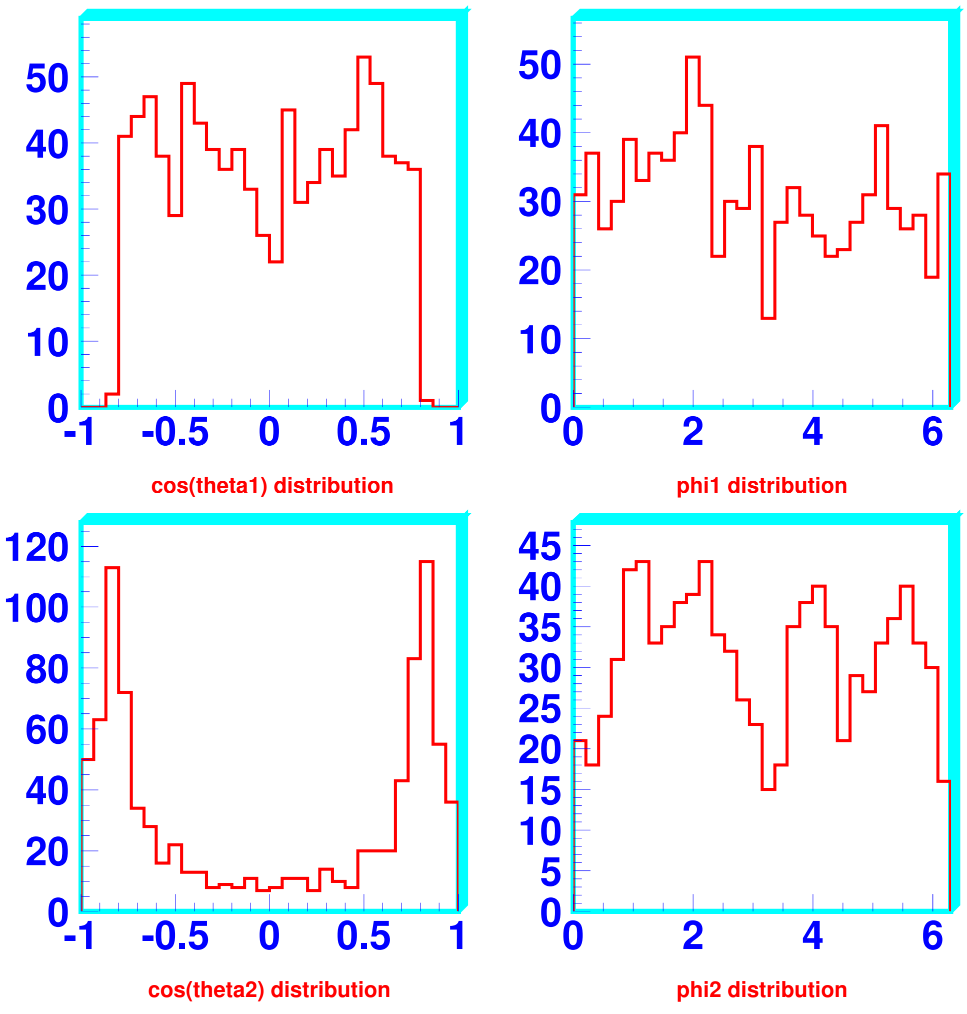

Figure 19: Angular distribution of BES data between 1.8 Gev — 2.1 Gev.

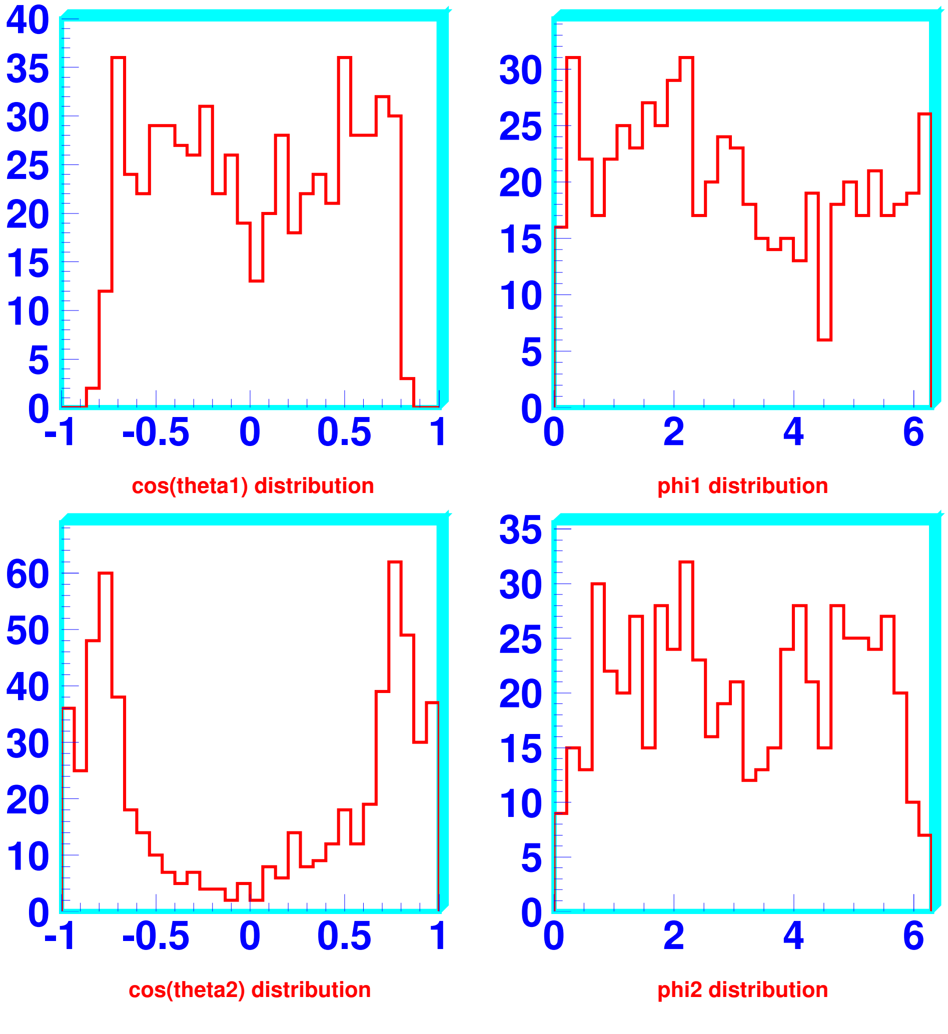

Figure 20: Angular distribution of BES data between 2.1 Gev — 2.3 Gev.

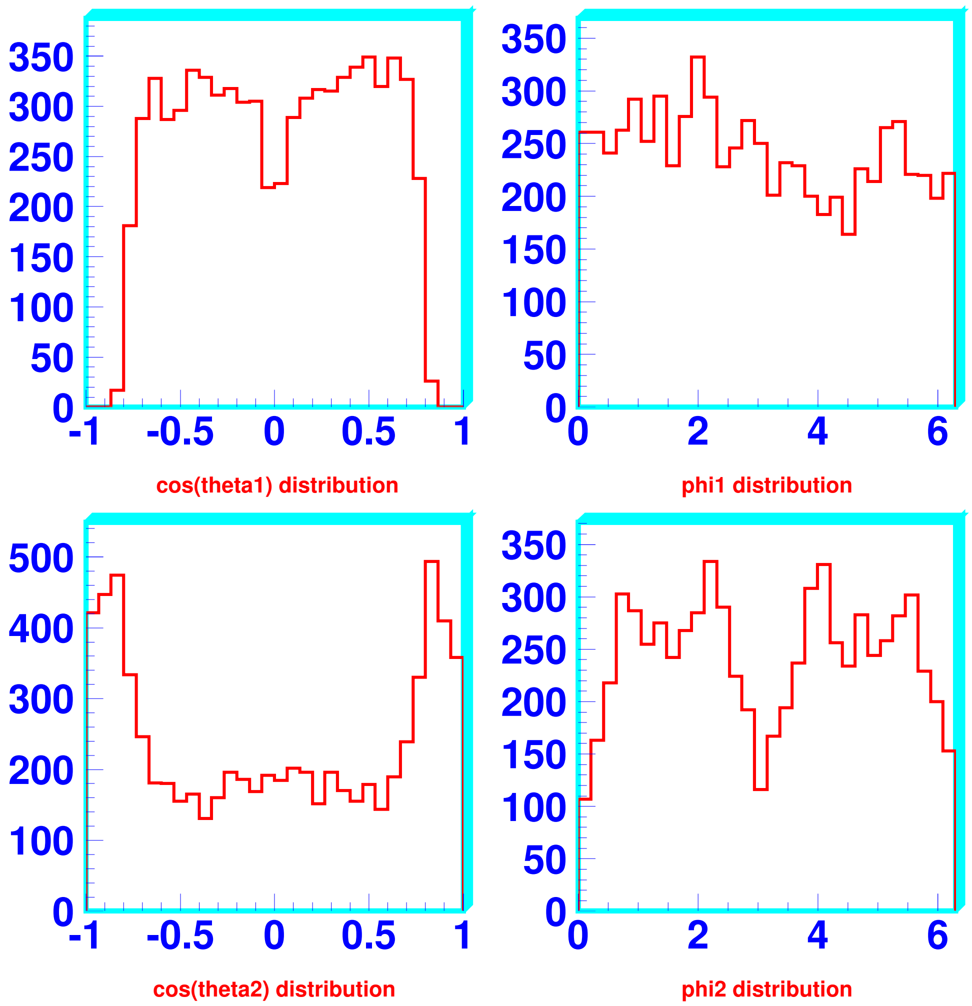

Figure 21: Angular distribution of BES data between 0.0 Gev — 2.3 Gev.

$J/\psi \to \rho\pi$, K^*K, γK^+K^-, $(n\gamma)e^+e^-$ and other $\pi^+\pi^-$ + neutrals. We did not make any further effort to reduce events coming from $J/\psi \to \rho\pi$, because the covariant helicity amplitude for $J/\psi \to \rho\pi$ can be written out and the contribution coming from $J/\psi \to \rho\pi$ can be calculated. In other words, $J/\psi \to \rho\pi$ is treated as if they were signal, not background events; this will be described in details below. Background events come from K^*K, γK^+K^- are also removed because we have used strong cut conditions to identify π and K. The background from radiative Bhabha events is removed by requiring that the angle between two charged tracks is less than 175° and the energy deposited in BSC of each charged track is less than $0.6Gev$. Background from $\pi^+\pi^-$ + neutrals is greatly reduced by requiring that the number of neutral tracks is 1, $\sin\alpha_1 \leq 0.15$ and $\chi^2_{4C}(\gamma\pi^+\pi^-) \leq 12.0$.

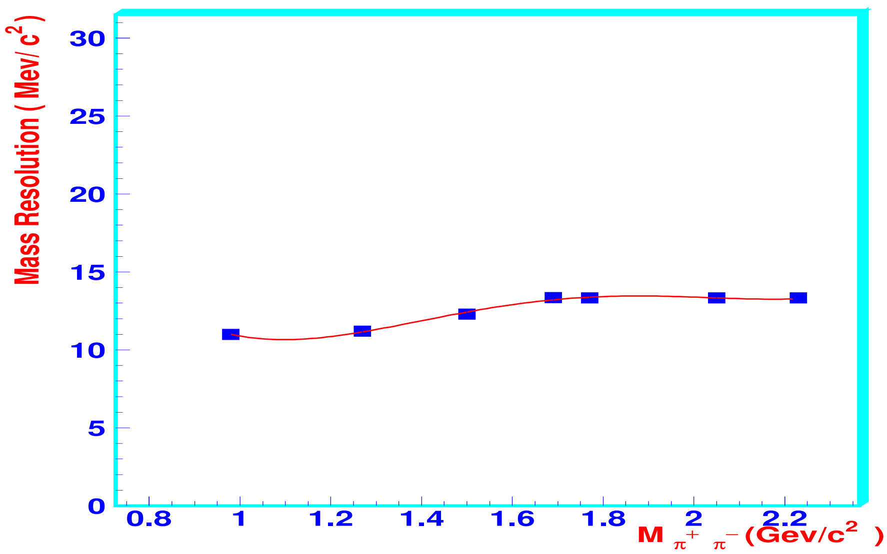

Figure 22: Mass resolution

The mass resolution for $J/\psi \to \gamma\pi^+\pi^-$ events in the whole mass region is shown in Fig.22 and the detection efficiency is shown in Fig.23. It can be seen that the detection efficiency is higher in the lower mass region and a little lower in the higher mass region. But changes are small over the whole mass region. The reason that detection efficiency decreases in the higher mass region is that, when the invariant mass of $\pi^+\pi^-$ is greater, the energy of the photon is smaller and then harder to detect. We use a polynomial of degree 4 to fit

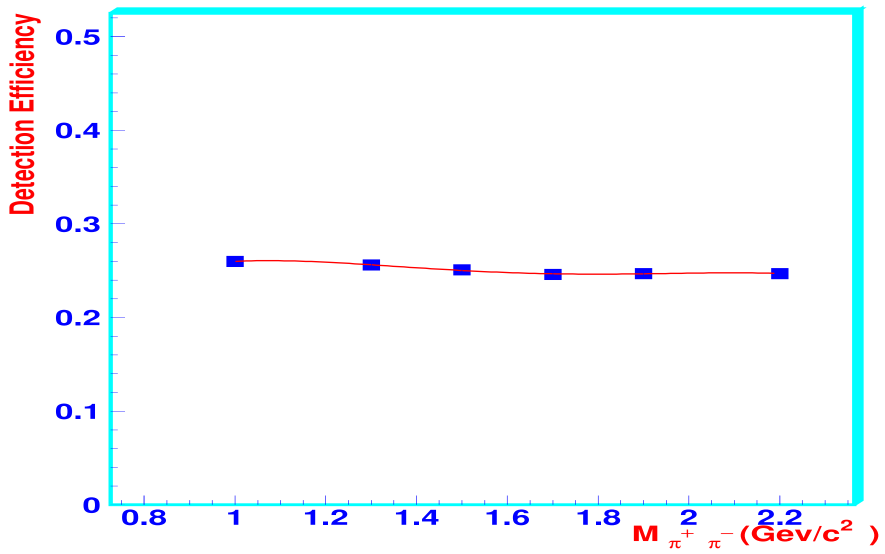

Figure 23: Detection efficiency

these points. The polynomial for detection efficiency EF is:

$$EF = -0.249 + 1.39 \times M - 1.37 \times M^2 + 0.57 \times M^3 - 0.086 \times M^4,$$

and the polynomial for mass resolution M_{reso} is:

$$M_{reso} = 97.0 - 230.43 \times M + 219.48 \times M^2 - 88.388 \times M^3 + 12.881 \times M^4,$$

with M the invariant mass of $\pi^+\pi^-$ in (Gev/c^2).

Analysis Method

The decay process $J/\psi \to \gamma\pi^+\pi^-$ is described by a sequential decay

$$\begin{array}{lllllll} J/\psi & \to & \gamma & + & X & & \\ & & & & \hookrightarrow & \pi^+ & + & \pi^-, \end{array}$$

where X is supposed to be a resonance with definite mass, with, spin and parity. In $J/\psi \to \gamma\pi^+\pi^-$, the possible spin-parity J^{PC} of X are 0^{++}, 2^{++}, 4^{++},$\cdots$.

The covariant helicity amplitude for this process consists of three parts: the covariant helicity amplitude describing the production process $J/\psi \to \gamma X$, the Breit-Wigner propagator of resonance X which contains the information on the mass and width of X, and the covariant helicity amplitude describing the decay process $X \to \pi^+\pi^-$.

There is a systematic way to calculate the covariant helicity amplitudes for two-body decay processes[17-20]; especially in reference [19-20], all covariant helicity amplitudes used in this work are listed. In the $J/\psi \to \gamma\pi^+\pi^-$ process, the following two-body decay processes are involved:

$$\begin{array}{cccc} 1^- & \to & 1^- & + & 0^+ \\ 1^- & \to & 1^- & + & 2^+ \\ 1^- & \to & 1^- & + & 4^+ \\ 0^+ & \to & 0^- & + & 0^- \\ 2^+ & \to & 0^- & + & 0^- \\ 4^+ & \to & 0^- & + & 0^- \end{array}$$

where the first three are radiative decays and the remaining three are non-radiative decays. Supposed that the spin-parity of the mother particle is $S_a^{\eta_a}$ and the spin-parity of two final state particles are $S_b^{\eta_b}$ and $S_c^{\eta_c}$ respectively. The helicities of two final state particles are λ_b and λ_c respectively. Then for a two-body decay process

$$\begin{array}{ccccc} a & \to & b & + & c \\ S_a^{\eta_a} & \to & S_b^{\eta_b} & + & S_c^{\eta_c}, \end{array}$$

the helicity coupling amplitude is usually denoted as:

$$M^{S_a}_{\lambda_b\lambda_c} \sim F^{S_a}_{\lambda_b\lambda_c} \cdot D^{S_a}_{\lambda_a(\lambda_b-\lambda_c)}.$$

All $F^{S_a}_{\lambda_b\lambda_c}$ used in this work can be found in [19]. The resonance X is described by a Breit-Wigner function $BW(s,m,\Gamma)$ with s the invariant mass square of $\pi\pi$, m the mass of X and Γ the width of X. In our fitting, we use a relativistic Breit-Wigner form:

$$BW(s,m,\Gamma) = \frac{-m\Gamma_{el}}{s - m^2 + im\Gamma},$$

where Γ_{el} is the partial width. Then the total covariant helicity amplitude for the sequential decay process $J/\psi \to \gamma X, \quad X \to \pi\pi$ is:

$$A_s = M^1_{1\ S} \cdot BW(s, m, \Gamma) \cdot M^S_{0\ 0},$$

where $M^1_{1\ S}$ is the helicity amplitude for $J/\psi \to \gamma X$, S is the spin of resonance X and $M^S_{0\ 0}$ is the helicity amplitude for $X \to \pi\pi$.

In addition, $J/\psi \to \rho\pi$ events exist in our data sample. The covariant helicity amplitudes for $J/\psi \to \rho\pi$ also can be written out, so we can also fit them as if they are useful events, not background events. This process consists of three decay processes:

$$J/\psi \to \rho^{\pm}\pi^{\mp} \quad and \quad \rho^0\pi^0,$$

$$\rho^{\pm} \to \pi^{\pm}\pi^0, \quad and \quad \rho^0 \to \pi^+\pi^-$$

$$\pi^0 \to \gamma\gamma.$$

In this process, two photon appear in the final state. But in our data selection, we select the events with only one good photon. So, in order to write out the amplitude for this process, we must find a way to calculate the energy-momentum of π^0. In our data selection, we have used a very strict cut condition on photon. We require that $\sin\alpha_1 \leq 0.15$; that means that the angle θ between the direction of the photon and $\vec{P}_{miss}$ is very small ($\theta < 8.5°$). If a π^0 decays into two photons and the angle between one of the photon and π^0 is very small, then the momentum of this photon will be very close to that of π^0 and the momentum of the other photon will be very small. In other words, the momentum of π^0 approximately equals to that of the photon whose moving direction is close to that of π^0. So, if a $J/\psi \to \rho\pi$ event survives our data selection, it must satisfy the following requirements: (1) π^0 decays into two photon, and the momentum of one of the photon is close to that of π^0's and the momentum of another photon is very small; (2) the photon with larger momentum is detected and is a good photon and the other photon is not detected. Denote the momentum of detected photons as $\vec{P}_\gamma$, then the following relation holds:

$$\vec{P}_{\pi^0} \approx \vec{P}_\gamma \ .$$

The energy of π^0 is calculate by the mass-energy relation:

$$E_{\pi^0} = \sqrt{\vec{P}^2_{\pi^0} + m^2_{\pi^0}}.$$

The covariant helicity amplitude for the sequential decay process $J/\psi \rightarrow \rho\pi, \quad \rho \rightarrow \pi\pi$ is:

$$A_{\rho\pi} = M^1_{1\ 1} \cdot BW(\rho) \cdot M^1_{0\ 0},$$

where $M^1_{1\ 1}$ is the helicity amplitude for $J/\psi \rightarrow \rho\pi$, $M^1_{0\ 0}$ is the helicity amplitude for $\rho \rightarrow \pi\pi$ and $BW(\rho)$ is the Breit-Wigner amplitude for the ρ.

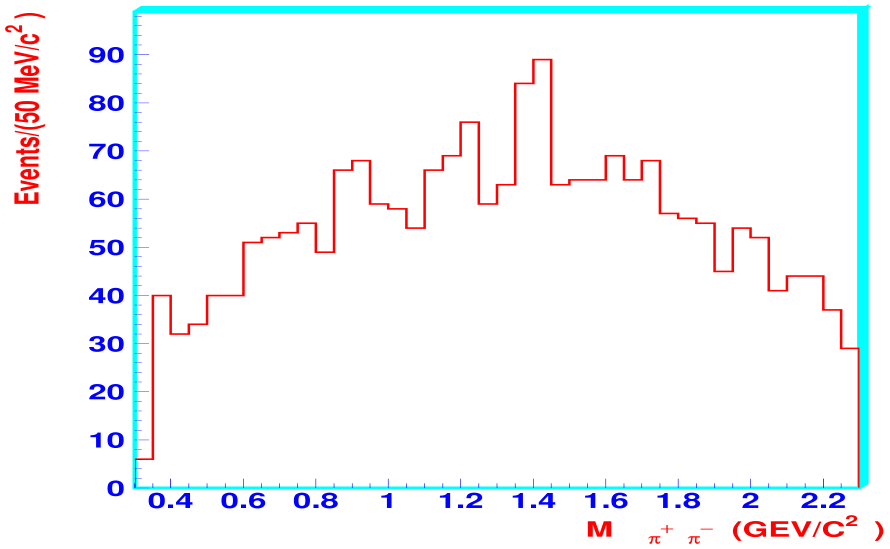

Figure 24: Invariant mass spectrum of $\pi^+\pi^-$ in $J/\psi \rightarrow \pi^0\pi^+\pi^-$ after final data selection.

There may also be some events come from direct three-body decays:

$$J/\psi \rightarrow \pi^0\pi^+\pi^-$$

and $\pi^+\pi^-$ + neutrals. For direct three-body decays $J/\psi \rightarrow \pi^0\pi^+\pi^-$, it is structureless and its distribution is similar to that of phase space which could be clearly seen from Fig.24 and Fig.25. The exact shape of the background coming form $\pi^+\pi^-$ + neutrals and from K^+K^- + neutrals is unpredictable and therefore hard to calculate strictly. But we can make some kind of approximation: we suppose that the shape of the $\pi^+\pi^-$ invariant mass spectrum coming from all background other than $\rho\pi$ is similar to that of phase space, so we use a phase space function to fit the contribution from all these backgrounds.

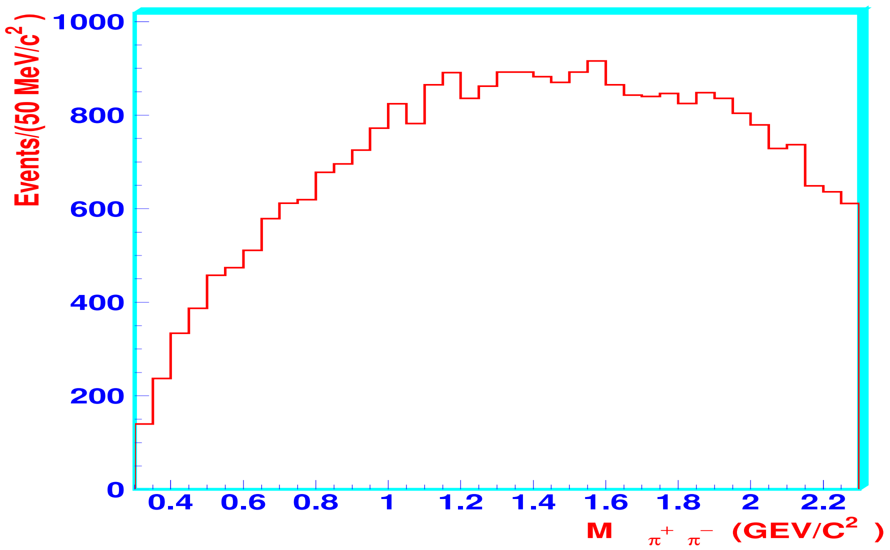

Figure 25: Phase space shape of $J/\psi \to \gamma\pi^+\pi^-$ after final data selection.

The total differential cross section is then given by:

$$\frac{d\sigma}{d\Phi} = \sum_{M\lambda_\gamma} |A_0 + A_2 + A_4 + \cdots|^2 + |A_{\rho\pi}|^2 + BG,$$

where

$$A_0 = A_0(980) + A_0(1500) + A_0(1770) + A_0(f_0(1030)) + \cdots$$

represents the total contribution from all 0^{++} resonances and

$$A_2 = A_2(1270) + A_2(1710) + A_2(2230) + \cdots$$

represents the total contribution from all 2^{++} resonances and

$$A_4 = A_4(2050) + \cdots$$

represents the total contribution from all 4^{++} resonances.

Maximum Likelihood Method is utilized in the fitting. Suppose that the probability density function $f(x, \alpha)$ that describe the data sample we have selected is:

$$f(x, \alpha) = \frac{d\sigma}{d\Phi}/\sigma$$

where x is a set of quantities that had been measured by experiment, such as 4-momenta of final state particles, α is a set of unknown parameters which needs to be determined in the fitting and σ is the total cross section of this process:

$$\sigma = \int \frac{d\sigma}{d\Phi} d\Phi.$$

It is given by Monte Carlo integration in the fitting:

$$\begin{aligned} \sigma &= \int \tfrac{d\sigma}{d\Phi} d\Phi \\ &= \tfrac{1}{N_{mc}} \sum_{i=1}^{N_{mc}} \left(\sum_{M\lambda_\gamma} |A_0 + A_2 + A_4 + \cdots|^2 + |A_{\rho\pi}|^2 + BG \right), \end{aligned}$$

where N_{mc} is the number of Monte Carlo events. The likelihood function $\mathcal{L}$ is given by the joint probability density of all experimental data:

$$\mathcal{L} = \prod_{i=1}^{N_{event}} f(x, \alpha).$$

In the Maximum Likelihood Method, the central task is to find the maximum of the likelihood function $\mathcal{L}$ by adjusting parameters α. If we define:

$$S = -\ln\mathcal{L},$$

then, finding the maximum of the likelihood function $\mathcal{L}$ will become finding the minimum of S. So, in the data fitting, the task is to find minimum of S by adjusting parameters α.

Analysis and Results

From the invariant mass spectrum of Fig.14 and the Dalitz plot, we may see strong contributions from $f_2(1270)$ and $\rho\pi$. Also a structure may exist in the mass region $1.7Gev$. Because $\rho\pi$ background was not completely removed, it is hard to clearly see any further structure from the mass spectrum by eye. Fortunately, we use more information of angular distributions as well as mass distributions in our analysis. That is, we can use the technique of mass and width scan to get more information on the structure in the mass spectrum.

After the analysis program is compiled, we firtst test our program on a known resonance. We test it on Monte Carlo data. Fig.26 shows the scan

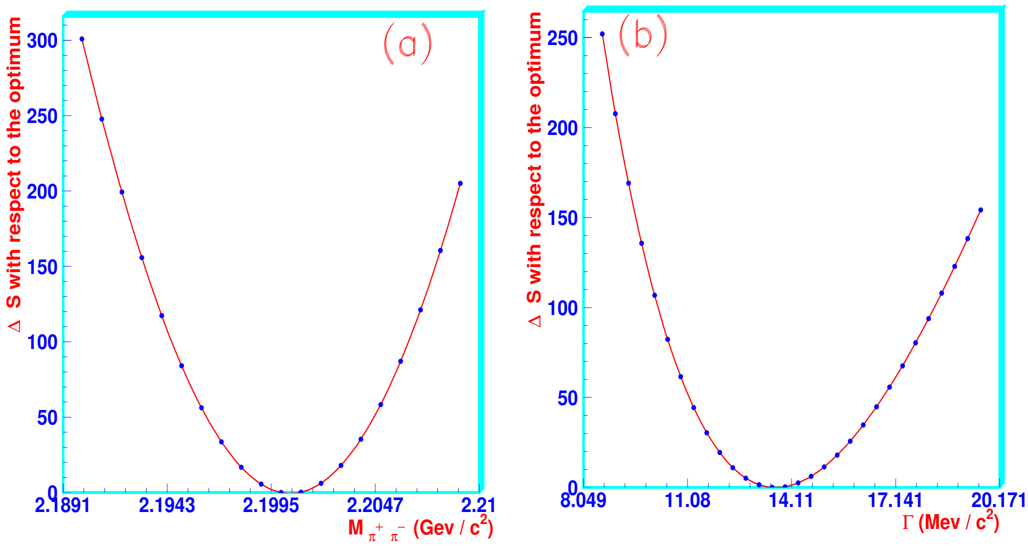

Figure 26: (a) Mass and (b) width scan on Monte Carlo data

results of Monte Carlo data with mass $2.2Gev$ and zero width. It shows a minimum at $M_{\pi\pi} = 2.20038Gev$ and $\Gamma = 13.68Mev$. This result is obtained by using a covariant helicity amplitude for a 0^{++} resonance, because the angular distribution of Monte Carlo data is similar to that of a 0^{++} resonance. Of course, Γ is the mass resolution at $2.2Gev$ for $J/\psi \to \gamma\pi^+\pi^-$. The width of the resonance can also be approximately estimated from mass scan results. If we use a Breit-Wigner function to fit the mass scan curve, we find that the width of this Breit-Wigner is about $13.66Mev$. In this simple case, the two methods give the same result. Because the width given by the width scan is more sensitive to statistical fluctuation, we can use this way to check the results given by the width scan and sometimes use it to determine the width. This test tell us that the program runs well in this simple case. We will use this program to analysis the structure of the mass spectrum of $\pi^+\pi^-$ in this channel.

The channel $J/\psi \to \gamma\pi^+\pi^-$ had been analyzed earlier by BES, MARK3 and DM2. From these works we know that the main resonances in this channel are $f_2(1270)$, $f_4(2050)$, and possibly $f_J(1710)$ and $f_J(2220)$. These resonances together with $\rho\pi$ background and a background which has the shape of phase

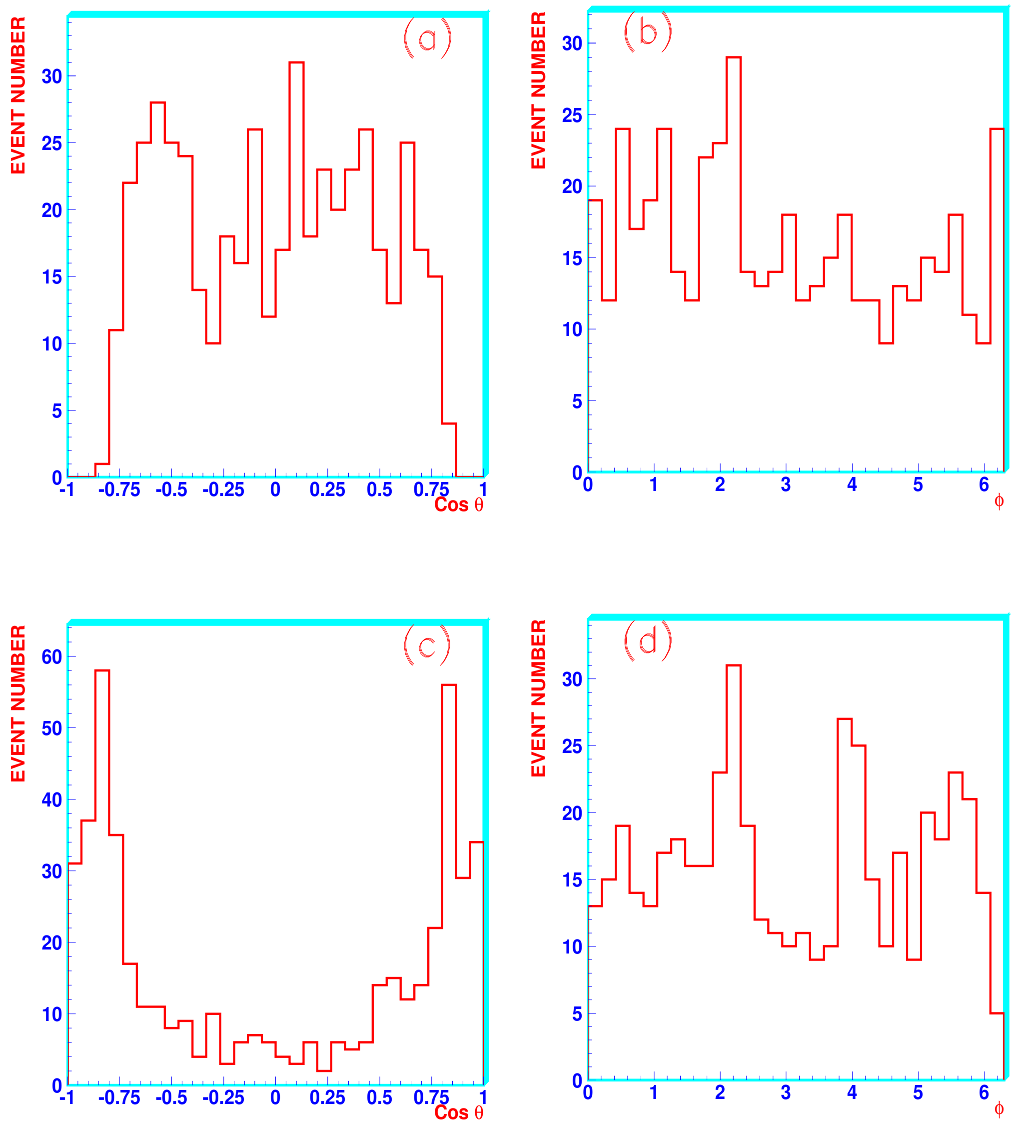

Figure 27: Angular distribution of real data in the 1.65-1.9 Gev region (a) and (b) is X's angular distribution in lab reference system and (c) and (d) is π^+ angular distribution in X's rest reference system.

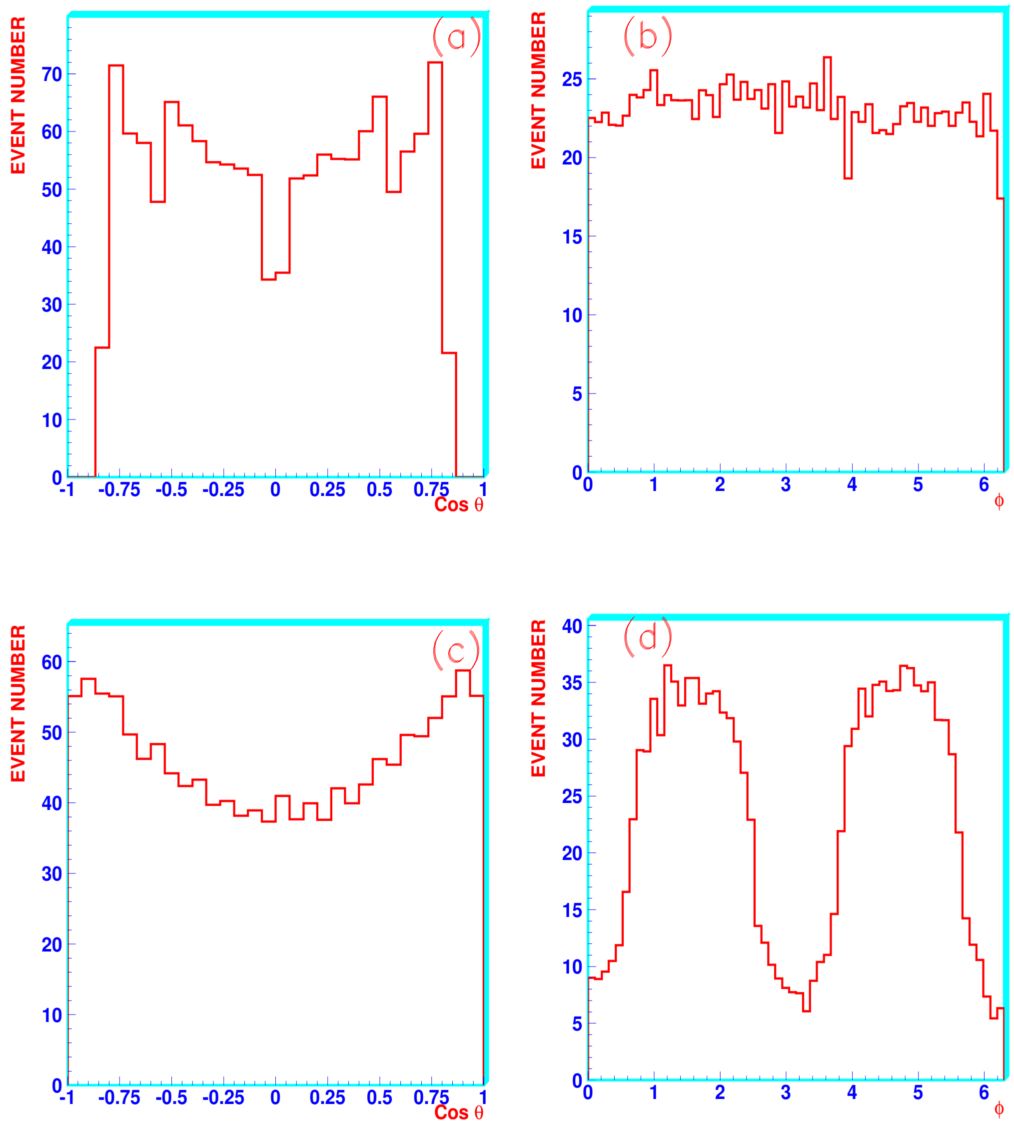

Figure 28: Angular distribution of Monte Carlo Projection for a 0^{++} (a) and (b) is X's angular distribution in lab reference system and (c) and (d) is π^+ angular distribution in X's rest reference system.

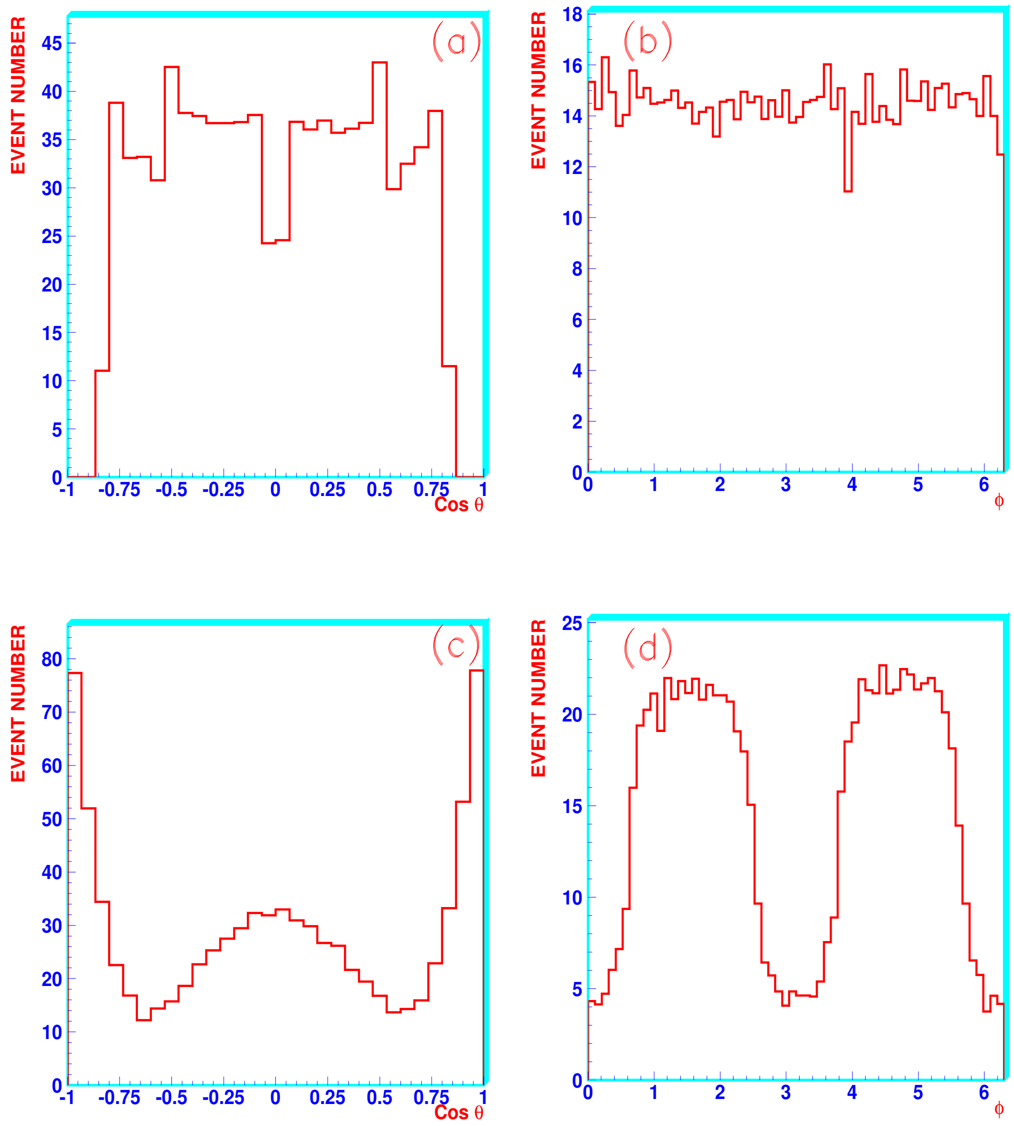

Figure 29: Angular distribution of Monte Carlo Projection for a 2^{++} (a) and (b) is X's angular distribution in lab reference system and (c) and (d) is π^+ angular distribution in X's rest reference system.

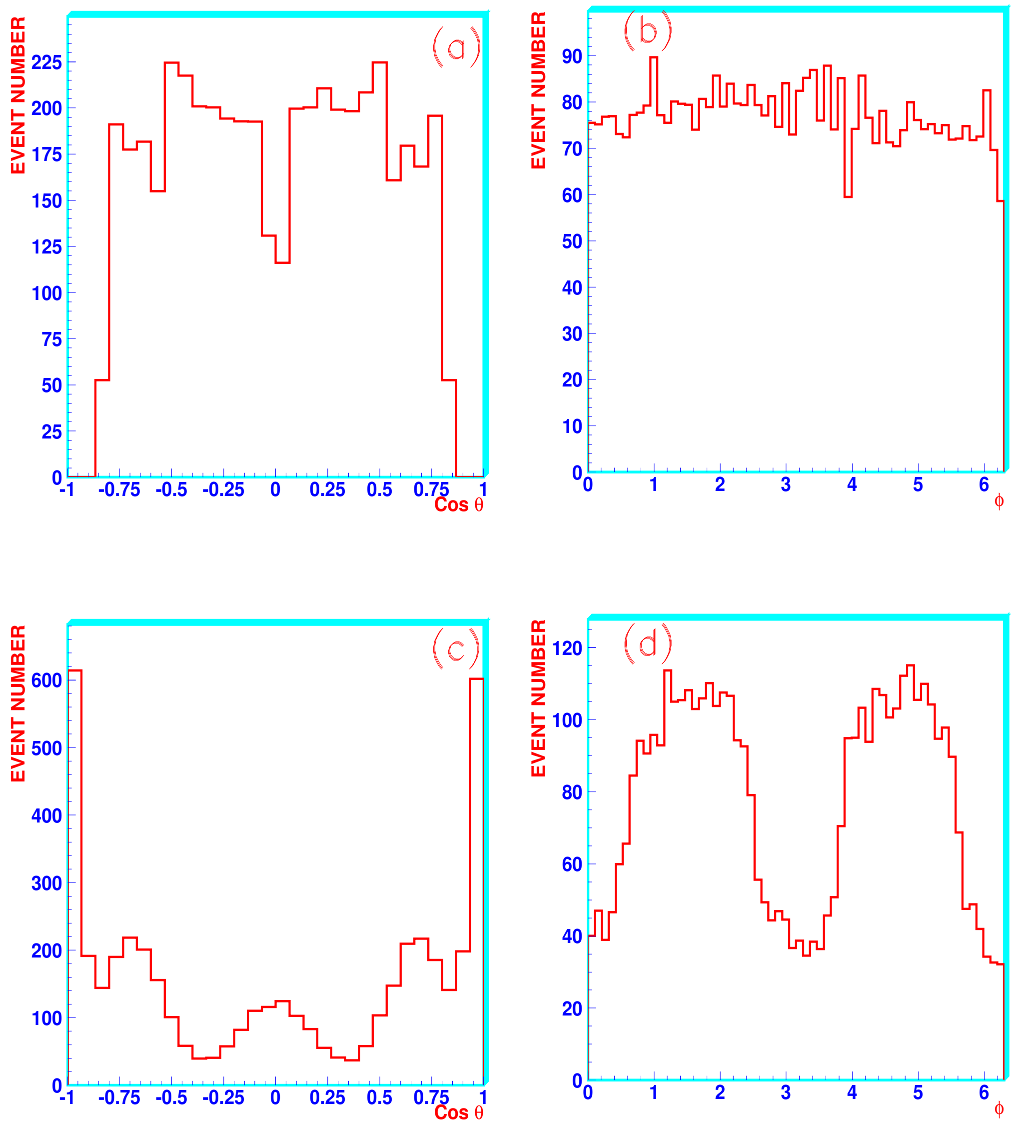

Figure 30: Angular distribution of Monte Carlo Projection for a 4^{++} (a) and (b) is X's angular distribution in lab reference system and (c) and (d) is π^+ angular distribution in X's rest reference system.

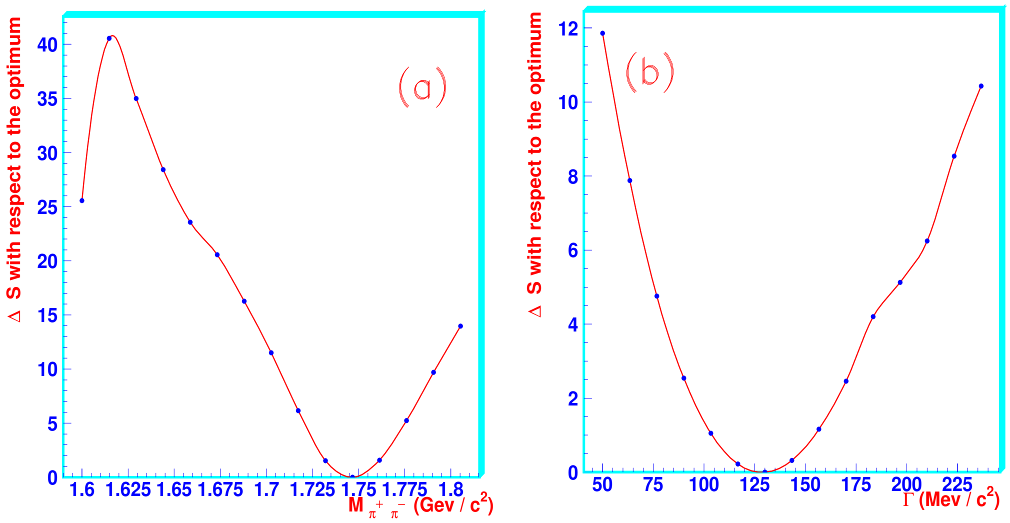

Figure 31: (a) Mass and (b) width scan on $f_0(1770)$ in $J/\psi \to \gamma\pi^+\pi^-$

space are first used in our initial global fitting of the data. Then, we find a broad 0^{++} resonance at about 1030 Mev by using the technique of mass and width scan. After that, we find that the our solution did not fit well in the $1.5Gev$ region. There is a dip in the real data. Therefore, we try to add a 0^{++} resonance here and find that destructive interference between $f_0(1500)$ and $f_0(1030)$ causes a dip which improves the fitting around $1.5Gev$ greatly. A similar case occurs in the $0.98Gev$ region, causing us to add $f_0(980)$ into our final solution.

resonances	$\Delta(\ln L)$	Effects
both 0^{++} and 2^{++}	0	—-
only 0^{++}(2 parameters)	26	6.9 σ
only 2^{++}(2 parameters)	12	4.5 σ

Table 3: Comparison among different alternatives.

It is known that an important issue is about the spin of $f_J(1710)$. Earlier

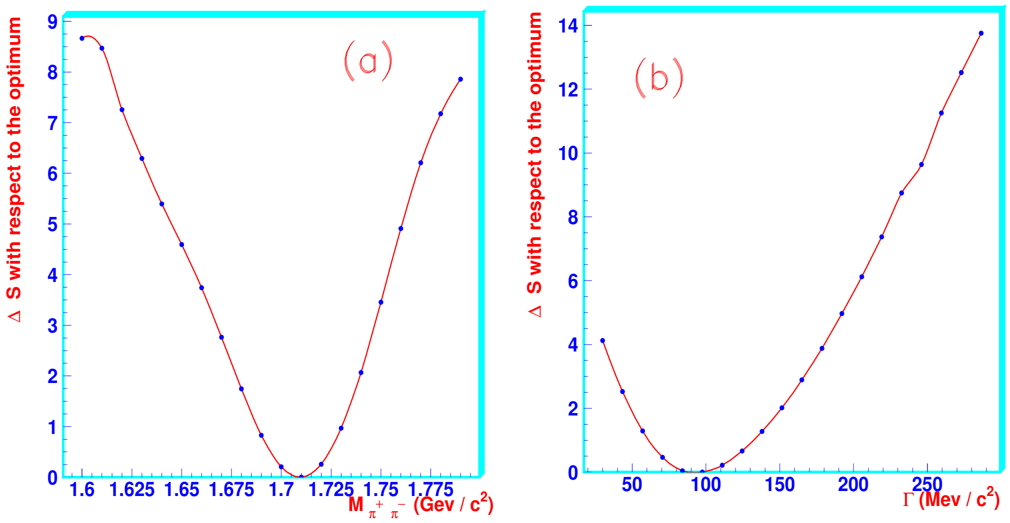

Figure 32: (a) Mass and (b) width scan on $f_2(1710)$ in $J/\psi \to \gamma\pi^+\pi^-$

J^P	M (MeV)	Γ_1 (MeV)	Γ_2 (Mev)
0^{++}	1747	130	~ 180
2^{++}	1710	98	~ 130

Table 4: Scan results around $1.71Gev$ region.

analysis favor spin 2, but some recent re-analysis favor spin 0. BES have ever done careful study on this region [15] and their results favor a spin 2 at about 1696 Mev and spin 0 at about 1781 Mev. Therefore, it is better not to make any prerequisite on the structure around 1.7 Gev region when we first begin to study this region and see our results favor which statements. We have done the follow things to study the structure here:

1. Because 0^{++} and 2^{++} has quite different angular distributions, we first see the angular distribution of real data in the 1.65-1.82 Gev region which is shown in Fig.27. As a comparison, the corresponding angular distributions for 0^{++}, 2^{++} and 4^{++} are shown in Fig. 28, Fig. 29 and Fig. 30 respectively. It could be seen that the angular distribution of real BES data does not like a pure 0^{++} at all, it is like a 2^{++}. It could be seen that strong contribution comes from 2^{++}. The structure in the 1.71 Gev region in the $\pi^+\pi^-$ channel is similar to that in the K^+K^- channel.

2. Mass scan is a strong and useful tool to study structure here. If only one 0^{++} exists in this region, when we use a 0^{++} to scan this region, we will find that the log likelihood drops greatly at this region while 2^{++} mass scan curve drops much less at the same position or it is just flat at this region. If only one 2^{++} exists in this region, the 2^{++} mass scan curve drops more at the pole than 0^{++}, and the minimum should be at the same position if 0^{++} mass scan curve has a minimu here. We first leave it blank and use a 2^{++} or 0^{++} resonance to scan this region. It has been done many times with different width or under some other different conditions. Every time, when we use a 2^{++} resonance to scan this region, the minimum of likelihood function is at about $1.71Gev$, and it is at about $1.75Gev$ when we use a 0^{++} resonance to scan this region. It means that at lower mass region, the angular distribution is more like a 2^{++} while at higher mass region, the angular distribution is more like a 0^{++}. These results obviously contradict with the hypothesis that only one 0^{++} or only one 2^{++} in this region.

3. If only one 0^{++} exists here and we have already added it into our solution, when we use another 0^{++} or 2^{++} to scan this region, we will find that the mass scan curve should be relatively flat. But, we find that only 0^{++} mass scan curve is flat, 2^{++} mass scan curve still has a deep dip here. Fig.32 is obtained in the condition that $f_0(1770)$ is already added into our solution. So, these scan results obviously contradict with the hypothesis that only one 0^{++} in this region.

4. If only one 2^{++} exists here and we have already added it into our solution, when we use another 2^{++} or 0^{++} to scan this region, we will find that the mass scan curve should be relatively flat. But, we find that only 2^{++} mass scan curve is flat, 0^{++} mass scan curve still has a deep dip here. Fig.31 is obtained in the condition that $f_2(1710)$ is already added into our solution. So, these scan results obviously contradict with the hypothesis that only one 2^{++} in this region.

5. The same procedure is done in $J/\psi \to \gamma K^+K^-$ and the results are the same. Furthermore, the masses of these two resonances obtained from mass scans are almost the same in these two channels. If only one resonance exists here, what cause this coincidence?

6. We use different resonances to fit this region. We have try four possibilities and list the results in Table 1. All changes in the magnitude of the likelihood function are relative to the case that both resonances are added in this region. In this test, we only open two dominant parameters to fit this region for both 0^{++} and 2^{++}. It is seen that without 0^{++}, log likelihood gets worse by 26, this is roughly a 6.9σ effect, while without 2^{++}, the log likelihood gets worse by 12, this is roughly a 4.5σ effect. It means that in this region, both 0^{++} and 2^{++} are needed for a good fit.

Obviously, all above results suggest that there are two resonance here. Fig.31 shows the change of the magnitude of the likelihood function in mass and width scans of $f_0(1770)$. Fig.32 shows those for $f_2(1710)$. In general, the magnitude of the likelihood function is much less sensitive to the change of width than to the change of mass. The width scan is more sensitive to statistical fluctuations of the mass spectrum and to nearby resonance. So the width of the resonance given by the width scan has larger fluctuations, especially in some regions with a complicated structure. Therefore, we always use mass scan results to estimate width. The scan results are listed in table 1, where Γ_1 is the result given by the width scan and Γ_2 is estimated from the mass scan. Acoording to our final results, the donminant component in this region is 0^{++}.

Another interesting region in this channel is around $1.5 Gev$. In the invariant mass spectrum, a dip rather than a peak is observed. In previous fit, no resonance exists here. But according to the PDG, the branching ratio of $J/\psi \to \gamma f_0(1500)$ is $(5.7 \pm 0.8) \times 10^{-4}$ and $f_0(1500)$ also decays into $\pi\pi$. These two results contradict with each other. Why is $f_0(1500)$ not seen in $J/\psi \to \gamma\pi^+\pi^-$? The reason is simple: it interferes destructively with other

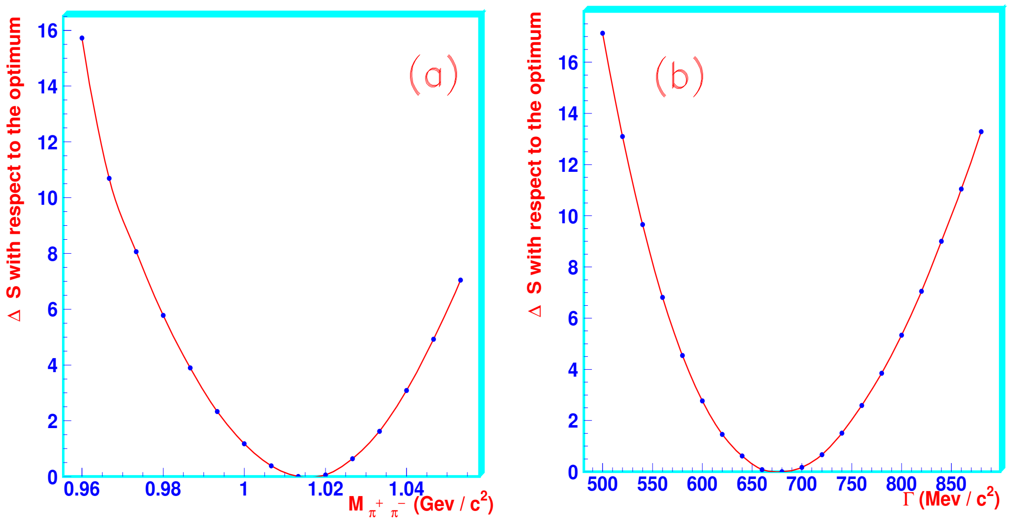

Figure 33: (a) Mass and (b) width scan on $f_0(1030)$ in $J/\psi \to \gamma\pi^+\pi^-$

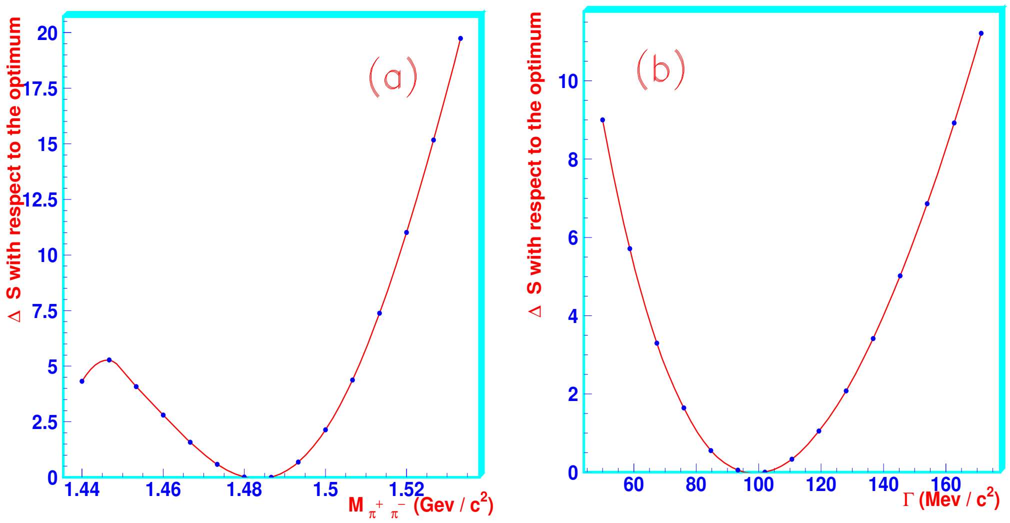

Figure 34: (a) Mass and (b) width scan on $f_0(1500)$ in $J/\psi \to \gamma\pi^+\pi^-$

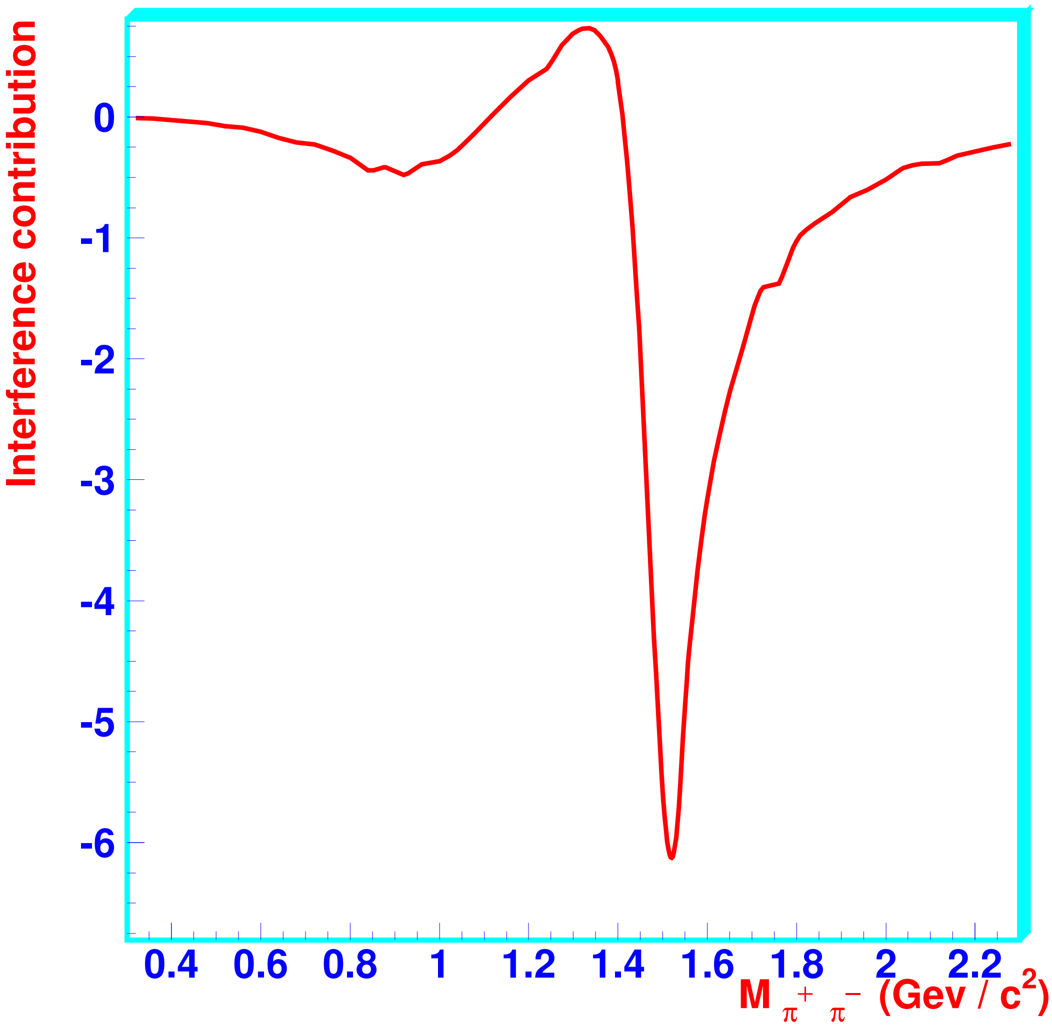

Figure 35: Interference between $f_0(1500)$ and $f_0(1030)$ in $J/\psi \to \gamma\pi^+\pi^-$

major components. In order to discuss $f_0(1500)$ in detail, let us first discuss another interesting 0^{++} resonance — $f_0(1030)$. Generally speaking, a very broad resonance does not show a peak in the mass spectrum, so we must be cautious when we add any broad resonance into our solution. We have done the following things on the studying of this broad resonance:

1. Initially, we did not add $f_0(1030)$ into our solution, because there is no peak corresponding to it. At this time, when we use a 0^{++} of about 100 Mev width to scan the whole mass region, we find that the mass scan curve shows two main dips at the lower mass region: one is above 0.98 Gev and another is below 0.98 Gev. These two dips are very wide, and a peak at about 0.98 Gev is between them. Besides, the mass scan curve has no dips at 1.5 Gev. One possibility is that there are two broad resonances in this channel, one is above 0.98 Gev, and another is below 0.98 Gev; $f_0(980)$ and $f_0(1500)$ do not present at this channel. But when we do mass and width scan on these two hypothesized resonance, we find that the mass scan curves are quite distorted, it does not like the standard mass scan curve at all. Furthermore, the width always becomes very large. If these two hypothesized resonances are real resonances, they must be affected by other resonances which make their width become larger and distort their mass scan curve.

2. If we do not add $f_0(1030)$ into our solution, when we do width scan on $f_0(1770)$, we find that its width is always very large. But from the mass scan curve, we could estimate that its width is not so wide. This phenomenon also occurs in $J/\psi \to \gamma K^+K^-$ channel. A possible explanation on this phenomenon is that there may be a very wide 0^{++} background, and, in order to fit 0^{++} components, the width becomes larger.

3. On the basis of the above conjecture, we use a very broad 0^{++} resonance to do mass scan in the whole mass range. Because the width is very broad, the scan can not "see" any structure that is much smaller than this width. In another word, any structure of about 100 Mev can not be seen by the scan. We found that the peak at 0.98 Gev in the previous mass scan curve disappear. Two big wide dips now joint together. It likes one broad resonance and the scan curves quite beautiful. Besides, the width given by width scan approximately equals to that estimated from mass scan. This result suggest that there is very broad 0^{++} background in this channel.

4. If we add this broad resonance 0^{++} into our solution and use another 0^{++} of about 100 Mev width to scan the whole mass region, we find that two former dips (one is above 0.98 Gev and another is below 0.98 Gev) disappear while the former peak at about 0.98 Gev now becomes an obvious dip. Another obvious dip appears at 1.5 Gev. These two dips are just at the positions of $f_0(980)$ and $f_0(1500)$. An explanation for this is that the interference between $f_0(980)$ and $f_0(1030)$ cause a dip of 0^{++} components at about 0.98 Gev (please see Fig.39(a)). If we do not add $f_0(1030)$ into our solution and use a 0^{++} to scan the whole mass region, we will find that there are two dip in the mass scan curve which corresponds to two humps of 0^{++} components in the lower mass region. We think that this explanation is more reasonable and we finally adopt this scenario. If we did not adopt this scenario, we will had to hypothesize that there are two resonances at about 0.9 Gev and 1.3 Gev respectively. At this time, in order to make width scan results more reasonable, we had to introduce a 0^{++} background. But after introduce this 0^{++} background, the two former 0^{++} resonances disappear. So, this hypothesis itself is not self-consistent.

5. We add this broad 0^{++} resonance into our solution and have done mass and width scan on it. The scan results are quite satisfactory which is shown in Fig.33. According to this scan, its mass and width should be $1017 Mev$ and $647 Mev$ respectively. Astonishingly, the same result is obtained independently in the $J/\psi \rightarrow \gamma K^+K^-$ channel[21]. This coincidence is absolutely not accidental phenomenon.

6. If we did not add this broad 0^{++} resonance into our solution, $f_0(980)$ and $f_0(1500)$ could not add into our solution too. After we add this broad 0^{++} resonance into our solution, $f_0(980)$ and $f_0(1500)$ must be added into our solution too, for the mass scan curve show very obviously big dips at 0.98 Gev and 1.5 Gev respectively. When we do mass scan on them, the results is quite close to those given by PDG. (see Figs. 34 and 38) If this broad 0^{++} resonance does not exist in this channel, how to explain the scan results on $f_0(980)$ and $f_0(1500)$?

7. If we delete this resonance, log likelihood will gets worse by 64; this is a 10.7σ effect.

In a word, $f_0(1030)$ is very important in the final solution and one of the biggest components in this channel, and also in $J/\psi \rightarrow \gamma K^+K^-$ channel. Because the $f_0(1030)$ is very broad, so it will have great interference with all other

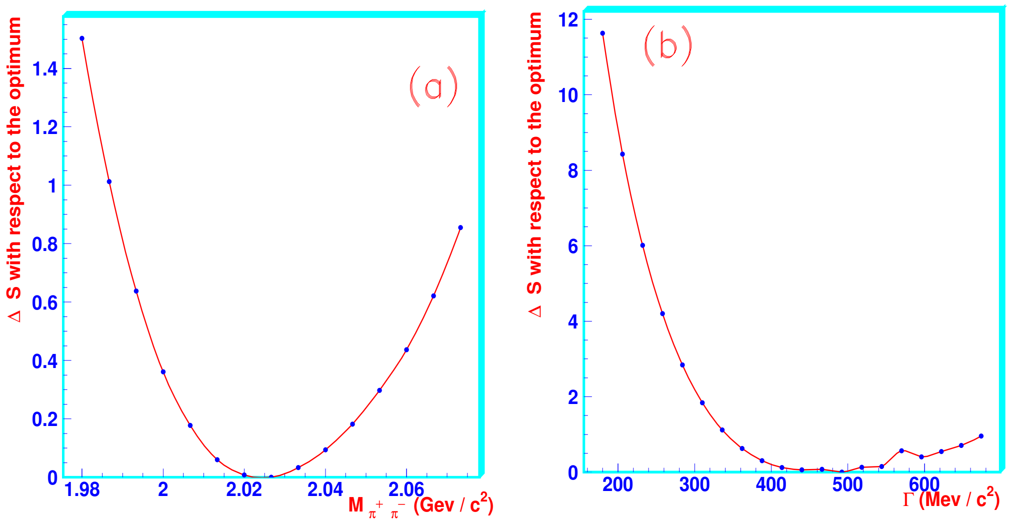

Figure 36: (a) Mass and (b) width scan on $f_4(2050)$ in $J/\psi \to \gamma\pi^+\pi^-$

0^{++} resonances. After we add interference between the $f_0(1030)$ and another 0^{++} resonance, we use this 0^{++} resonance to scan the $1.5Gev$ region. We got a surprising discovery: a resonance exists in the dip! Fig.34 shows the scan results. It can be seen that $f_0(1500)$ is very obvious. It improves log likelihood by about 46, which corresponds to a 8.9σ effect. So, it is also very important to the final solution. According to this scan, the mass and width of $f_0(1500)$ are 1490 Mev and 102 Mev respectively. From Monte Carlo projection of the final solution, we do see a dip in $1.5Gev$ region which is caused by interference between $f_0(1500)$ and the $f_0(1030)$. The shape of the interference between $f_0(1500)$ and $f_0(1030)$ is shown in Fig.35, which is the Monte Carlo projection of the final solution. From this figure, we see that almost in the whole range, the interference between $f_0(1500)$ and $f_0(1030)$ is destructive, so the phase difference between two resonance is about $180°$. It creates a dip around $1.5Gev$ and explains why a dip at $1.5Gev$ corresponds to a resonance and why we could not see a peak in the mass spectrum corresponding to $f_0(1500)$ in the $J/\psi \to \gamma\pi^+\pi^-$ channel.

According to the PDG, there is a 4^{++} resonance at $2.05Gev$. We add this resonance into our solution and its scan results are shown in Fig.36. According

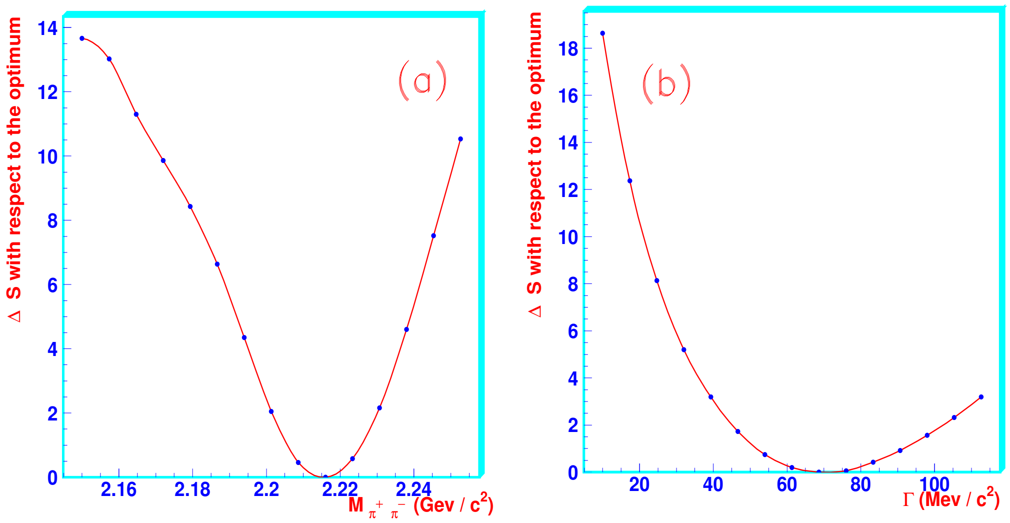

Figure 37: (a) Mass and (b) width scan on $f_2(2230)$ in $J/\psi \to \gamma\pi^+\pi^-$

to this scan, its mass and width are about $2.041 Gev$ and $???Mev$ respectively. If we omit this resonance, the log likelihood will become worse by about 52 which corresponds to a 9.5σ effect.

resonances	$\Delta(\ln L)$
no resonance here	0
only 0^{++}	-6
only 2^{++}	-25
only 4^{++}	-21

Table 5: Comparison among different alternatives.

Now, let's turn to the $2.2Gev$ region. According to previous BES results, there should be a narrow 2^{++} resonance here. Because $\rho\pi$ is treated as a signal in our analysis and we did not do much further effort to cut $\rho\pi$, we could not see an obvious peak here. But this does not affect our analysis, for $\rho\pi$ and a 2^{++} resonance have quite different angular distribution. We have used 0^{++},

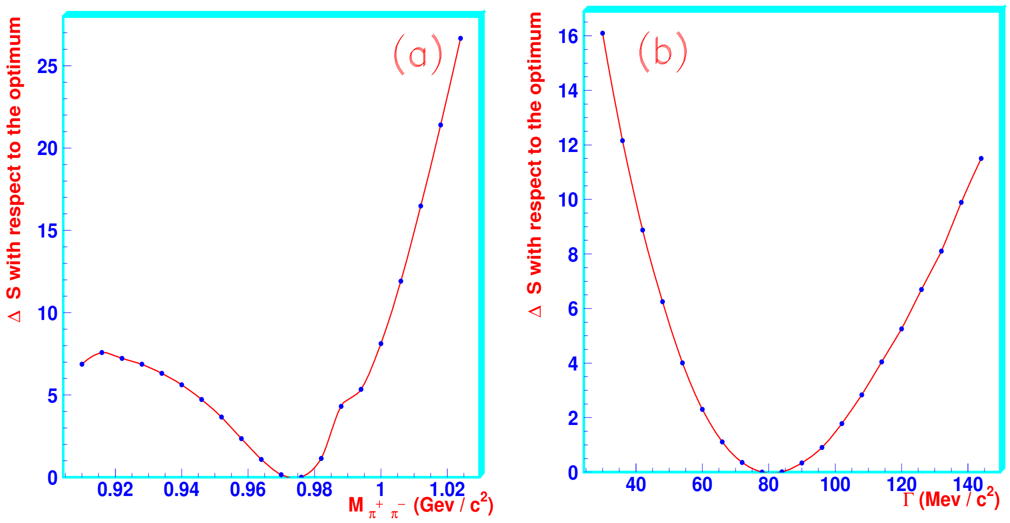

Figure 38: (a) Mass and (b) width scan on $f_0(980)$ in $J/\psi \to \gamma\pi^+\pi^-$

2^{++} and 4^{++} resonances to scan this region, and found that only 2^{++} shows a clear dip here. Besides, we have seen which improve the log likelihood most. Results are listed in table 3. So, this resonance is most like a 2^{++} resonance and most unlike a 0^{++}. But the statistics here is not enough to differentiate 2^{++} from 4^{++}. We use a 2^{++} to fit this region. The mass and width scan curves are quite beautiful and standard curves, which is shown in Fig.37. According to this scan, its mass and width are 2216 Mev and 69 Mev respectively. From the mass scan curve, it could be estimated that its width is also very narrow. So, this resonance is not the wide resonance $f_2(2150)$ whose width is $150 Mev$.

Finally, we turn to the $1.0 Gev$ region. A clear dip exist here in the invariant mass spectrum. But this situation is similar to that of the $1.5 Gev$ region. It is natural to guess that this dip is created by interference between $f_0(980)$ and $f_0(1030)$. We have tried this possibilities and used a narrow 0^{++} resonance to scan this region. Fortunately, our conjecture comes true again. A narrow 0^{++} resonance is found here. We also do mass and width scans on it routinely and the scan results are shown in Fig.38. According to this scan, its mass and width are 975 Mev and 78 Mev respectively. The interference between $f_0(980)$ and $f_0(1030)$ is shown in Fig.39. It can be seen that the interference

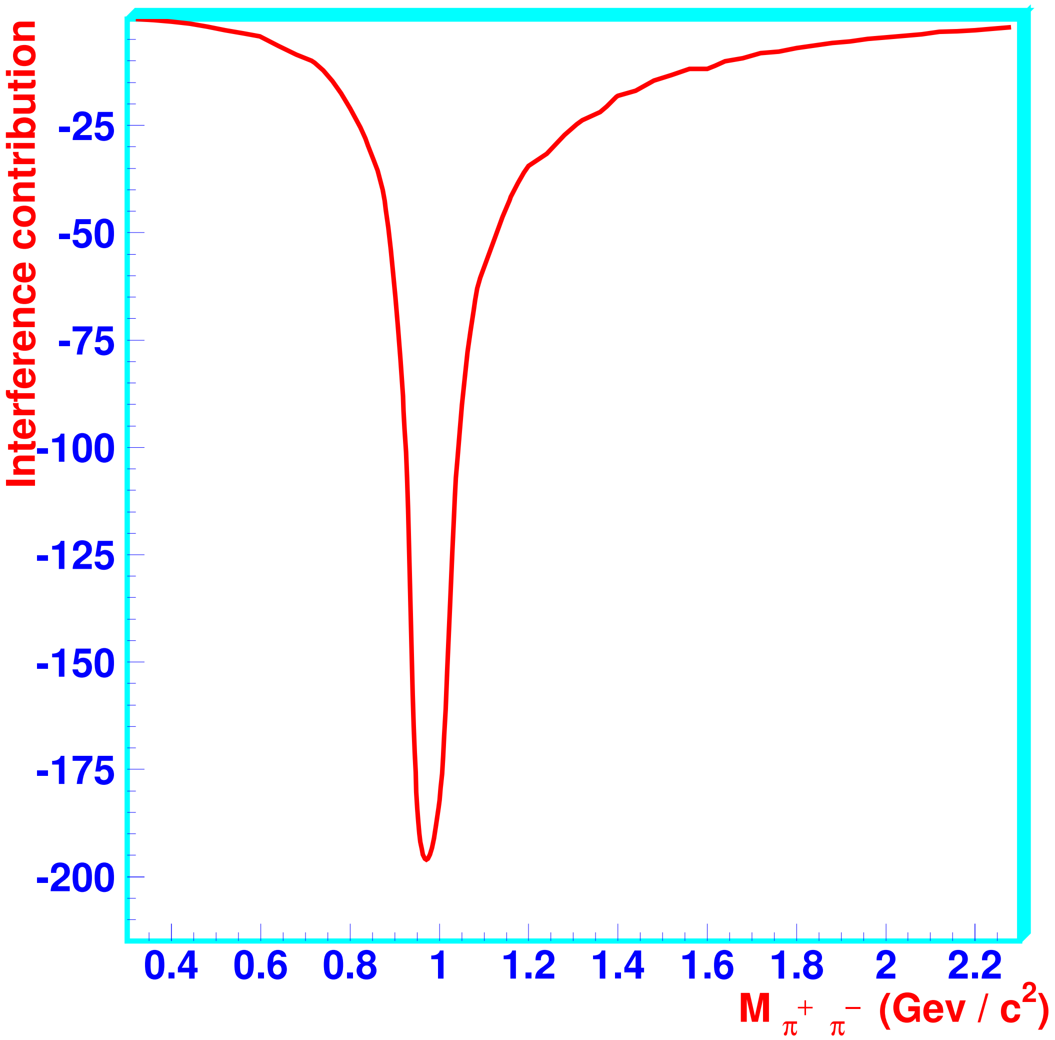

Figure 39: Interference between $f_0(980)$ and $f_0(1030)$ in $J/\psi \to \gamma\pi^+\pi^-$

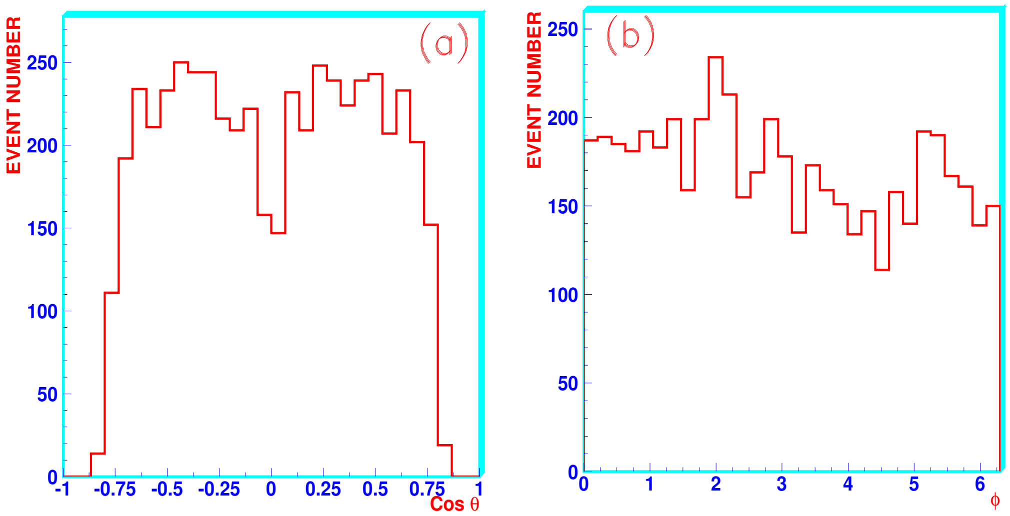

Figure 40: X's Angular distribution of real data

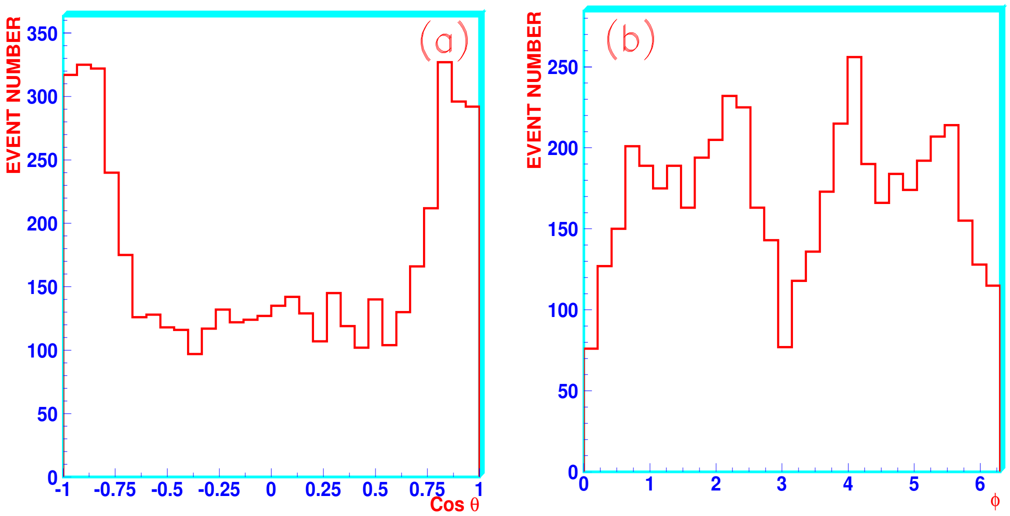

Figure 41: π^+ Angular distribution of real data

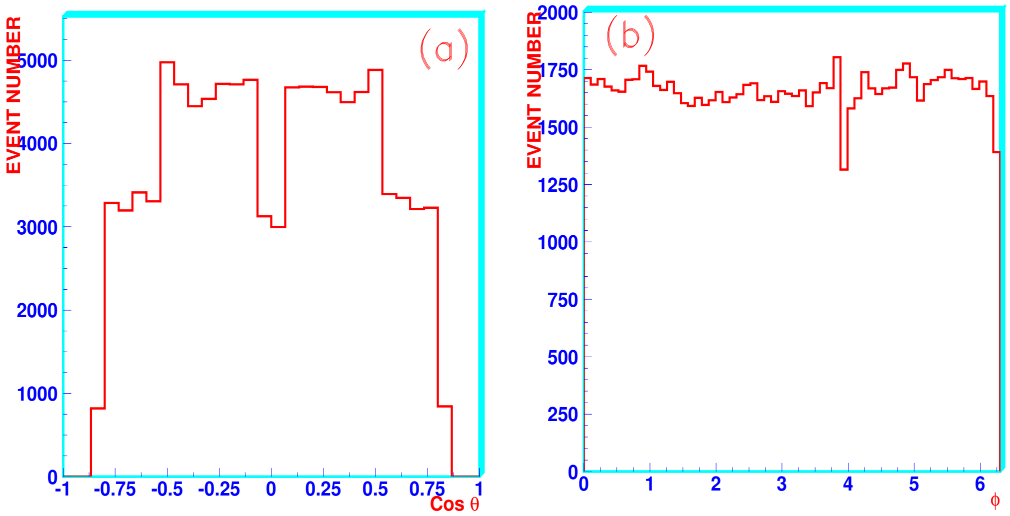

Figure 42: X's Angular distribution of Monte Carlo projection

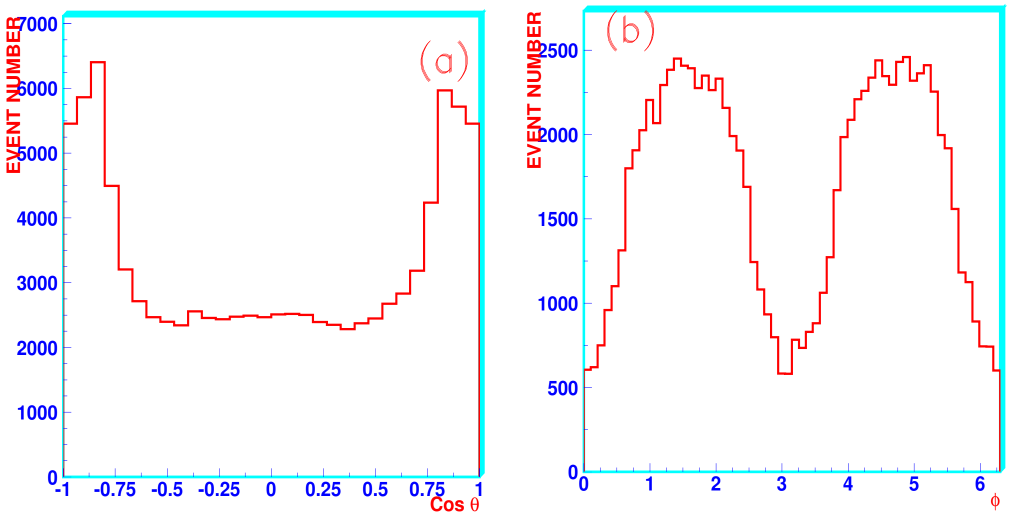

Figure 43: π^+ Angular distribution of Monte Carlo data

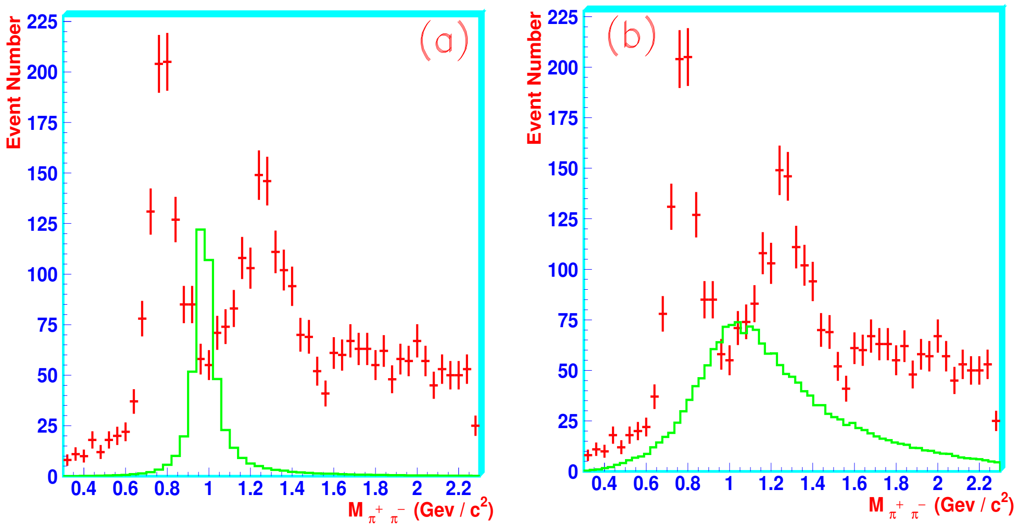

Figure 44: Contribution from (a) $f_0(980)$ and (b) $f_0(1030)$.

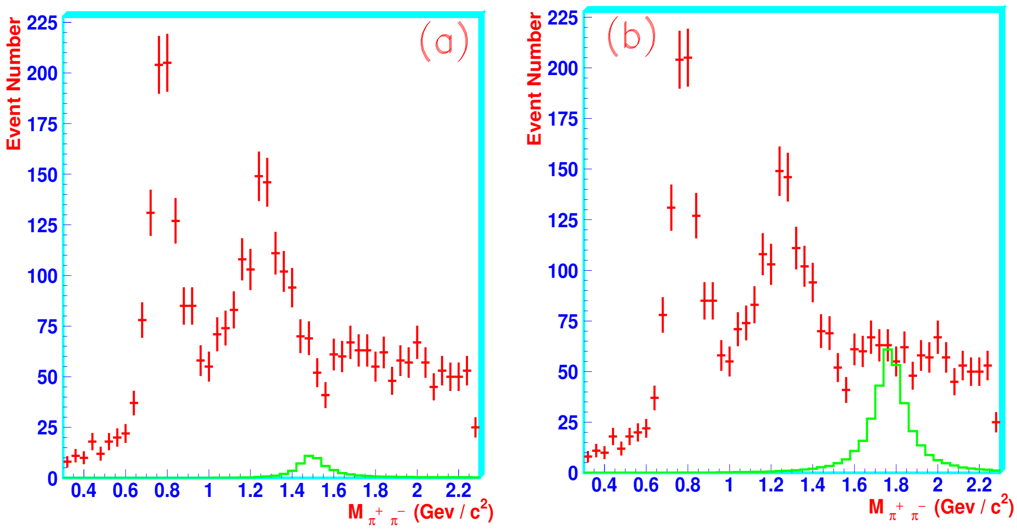

Figure 45: Contribution from (a) $f_0(1500)$ and (b) $f_0(1770)$

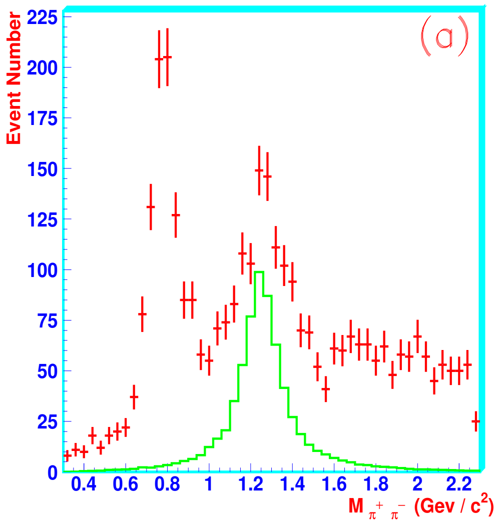

Figure 46: Contribution from (a) $f_2(1270)$ and

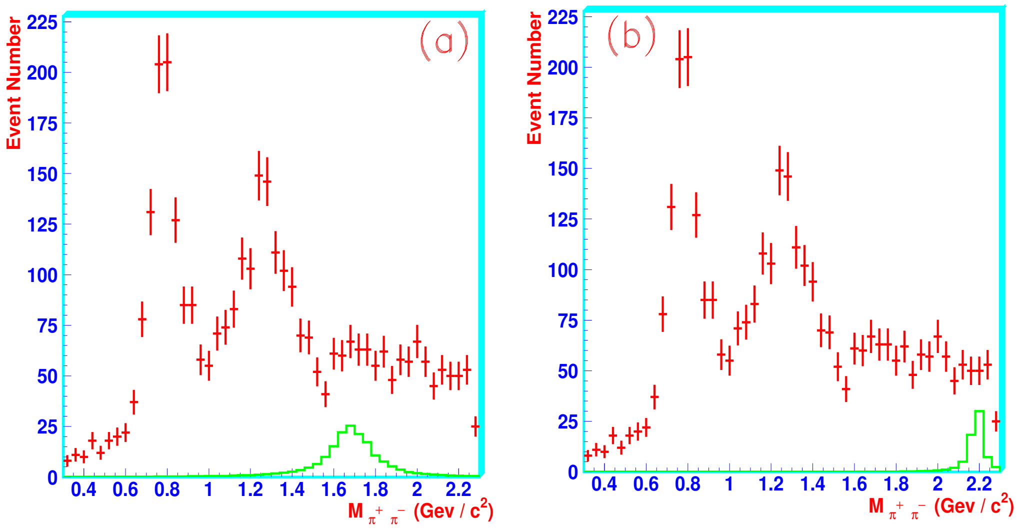

Figure 47: Contribution from (a) $f_2(1710)$ and (b) $f_2(2230)$

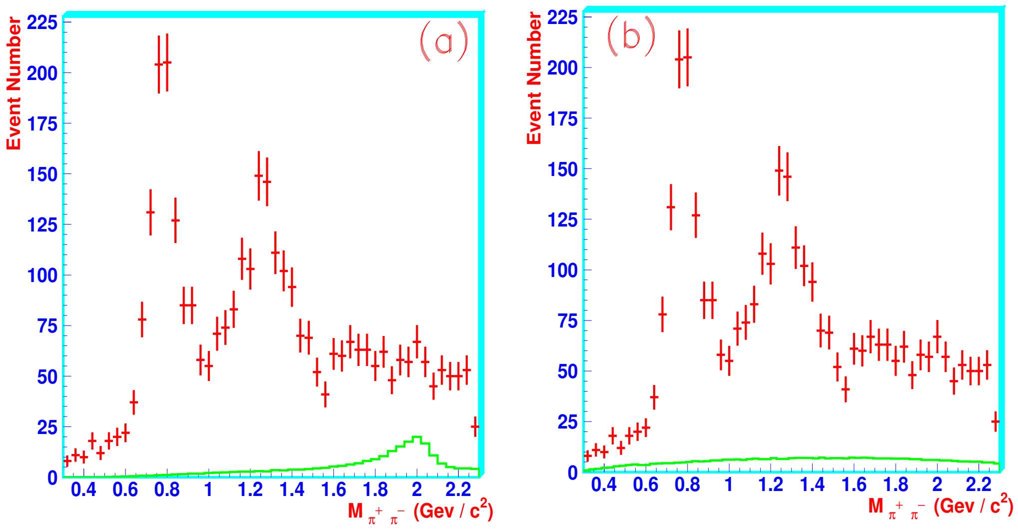

Figure 48: Contribution from (a) $f_4(2050)$ and (b) background

in the whole region is destructive. This is the reason we could not see the peak of $f_0(980)$ in the $\pi^+\pi^-$ invariant mass spectrum in this channel. It should be noted that it is generally believed that $f_0(980)$ is not produced in radiative J/ψdecays. It is also generally believed that it is not an ordinary meson. And because $f_0(980)$ was not produced in radiative J/ψ decay, it was believed that it is not a candidate of scalar glueball. Now, according to our new analysis results on $J/\psi \to \gamma\pi^+\pi^-$ and $J/\psi \to \gamma K^+K^-$, $f_0(980)$ is abundantly produced in radiative J/ψ decay, so it is natural to regard it as an important candidate of scalar glueball or at least a state containing a scalar glueball component.

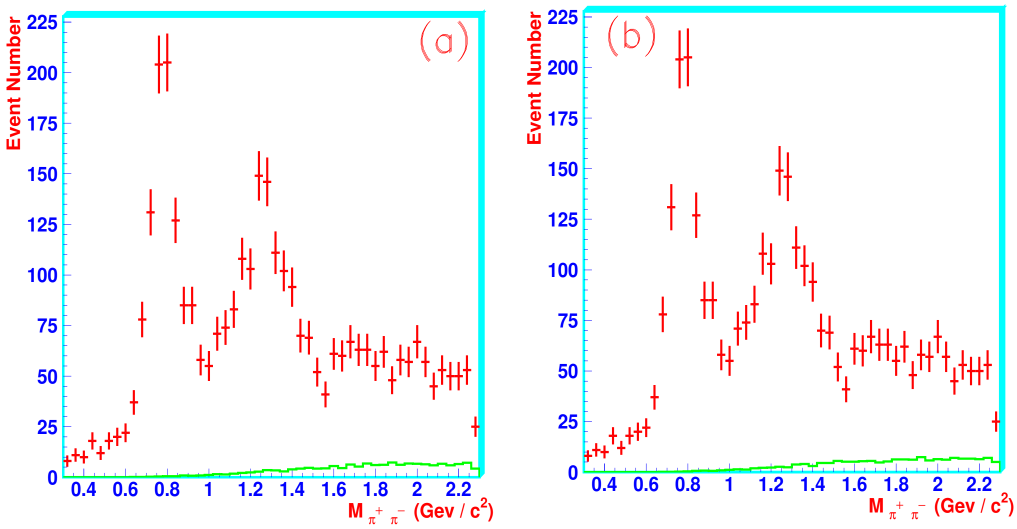

Figure 49: Contribution from (a) $\rho^-\pi^+$ and (b) $\rho^+\pi^-$

Our final fit uses all above resonances together with $\rho\pi$ background and a background which has the shape of phase space (used to describe contributions comes from all other backgrounds). After obtaining the final solution, we could see the quality of fitting through comparing different distributions of real data and Monte Carlo projection of the final solution. The angular distribution of real data is shown in Fig.40 and Fig.41. Fig.40 shows the polar angular distribution and azimuthal angular distribution of X, where X is the resonance which will decay into $\pi^+\pi^-$. Fig.41 shows the polar angular distribution and azimuthal angular distribution of π^+ in the rest frame of X. The corresponding Monte Carlo projection is shown in Fig.42 and Fig.43. It can be seen that the angular distribution of real data and Monte Carlo projections are quite similar. Figs.44–51 show contributions come from a separate resonance while Figs.53–57 show the shape of some interferences. Figs.53—57 just show the shape of interference. We did not normalize them to the real contributions. Finally, Fig.58 shows the global fitting.

In our final solution, the following resonances are included: $f_0(980)$, $f_0(1030)$, $f_2(1270)$, $f_0(1500)$, $f_2(1710)$, $f_0(1770)$, $f_4(2050)$ and $f_2(2230)$. Their masses and widths are listed in table 4 and their branching ratios in table 5. The branch ratio given here is $BR(J/\psi \to \gamma X) \times BR(X \to \pi^+\pi^-)$.

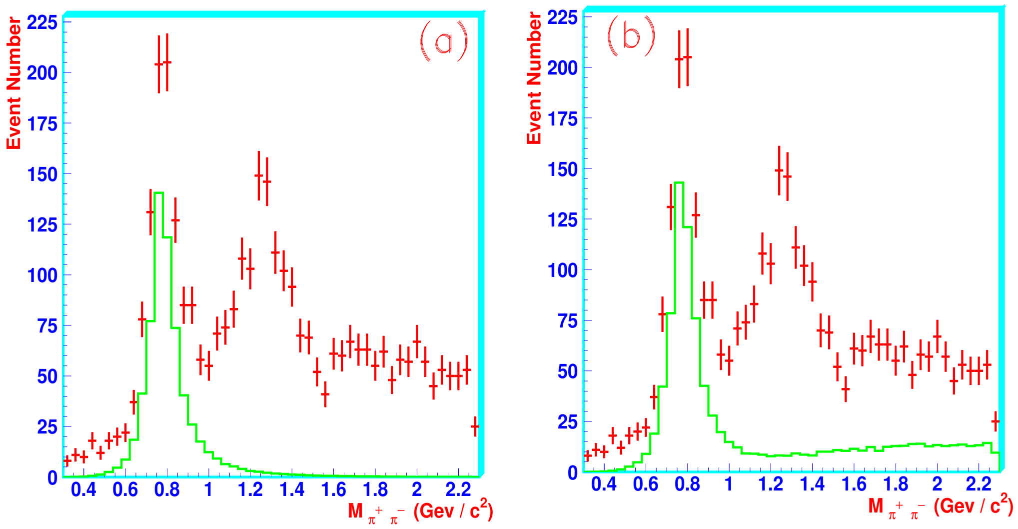

Figure 50: Contribution from (a) $\rho^0\pi^0$ and (b) total $\rho\pi$

resonances	Mass (Mev)	Width (Mev)	$\Delta(\ln L)$	Effects
$f_0(980)$	975^{+10}_{-15}	78^{+28}_{-18}	34	7.5 σ
$f_0(1030)$	1017^{+16}_{-24}	647^{+120}_{-90}	64	10.7 σ
$f_2(1270)$	1257^{+24}_{-22}	205^{+50}_{-35}	63	10.6 σ
$f_0(1500)$	1490^{+13}_{-30}	102^{+28}_{-29}	46	8.9 σ
$f_2(1710)$	1710^{+33}_{-36}	98^{+60}_{-55}	12	3.9 σ
$f_0(1770)$	1747^{+23}_{-20}	130^{+43}_{-40}	26	6.4 σ
$f_4(2050)$	2027^{+85}_{-75}	490^{+300}_{-270}	52	9.5 σ
$f_2(2230)$	2216^{+16}_{-20}	69^{+43}_{-38}	25	6.3 σ

Table 6: Mass, Width and statistical significance for various resonances.(Errors correspond to one σ variations.)

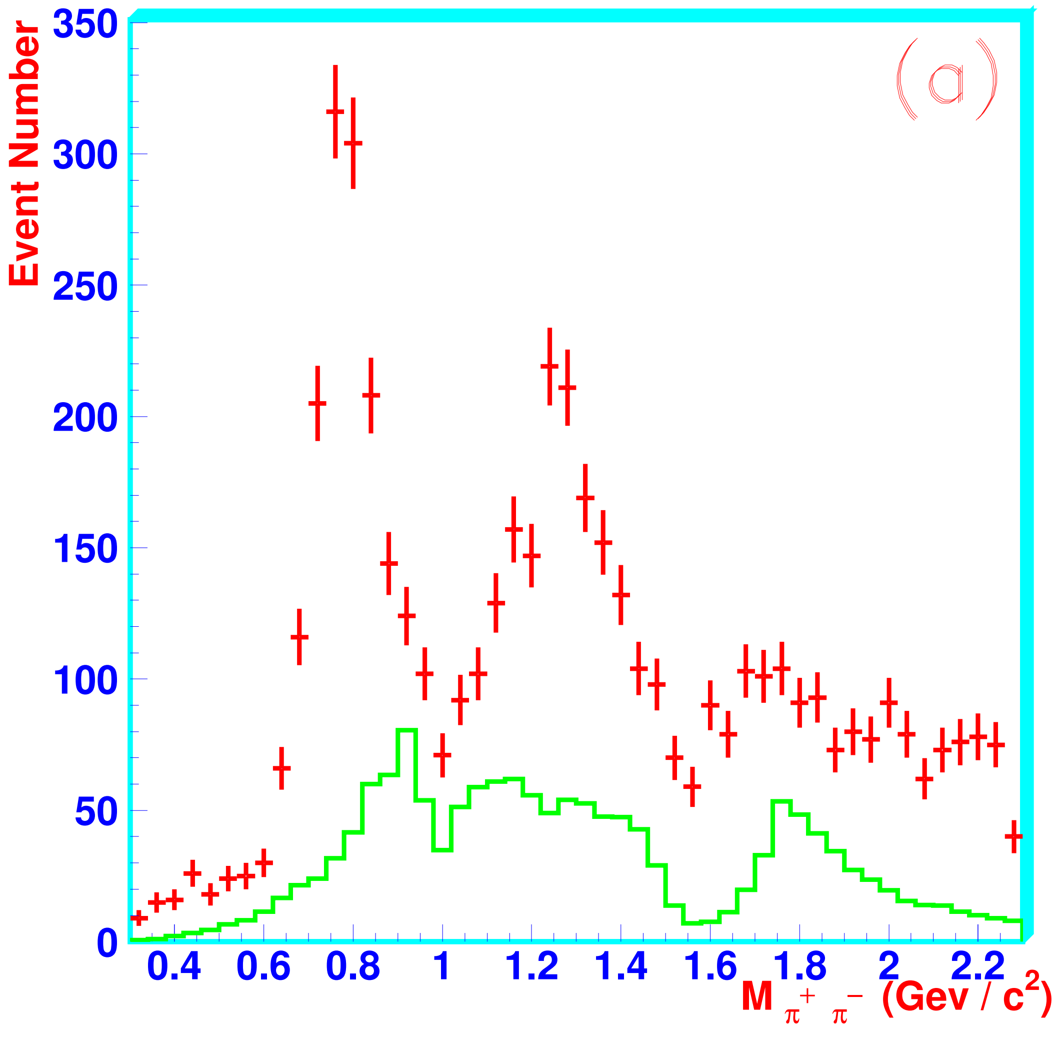

Figure 51: Total 0^{++}

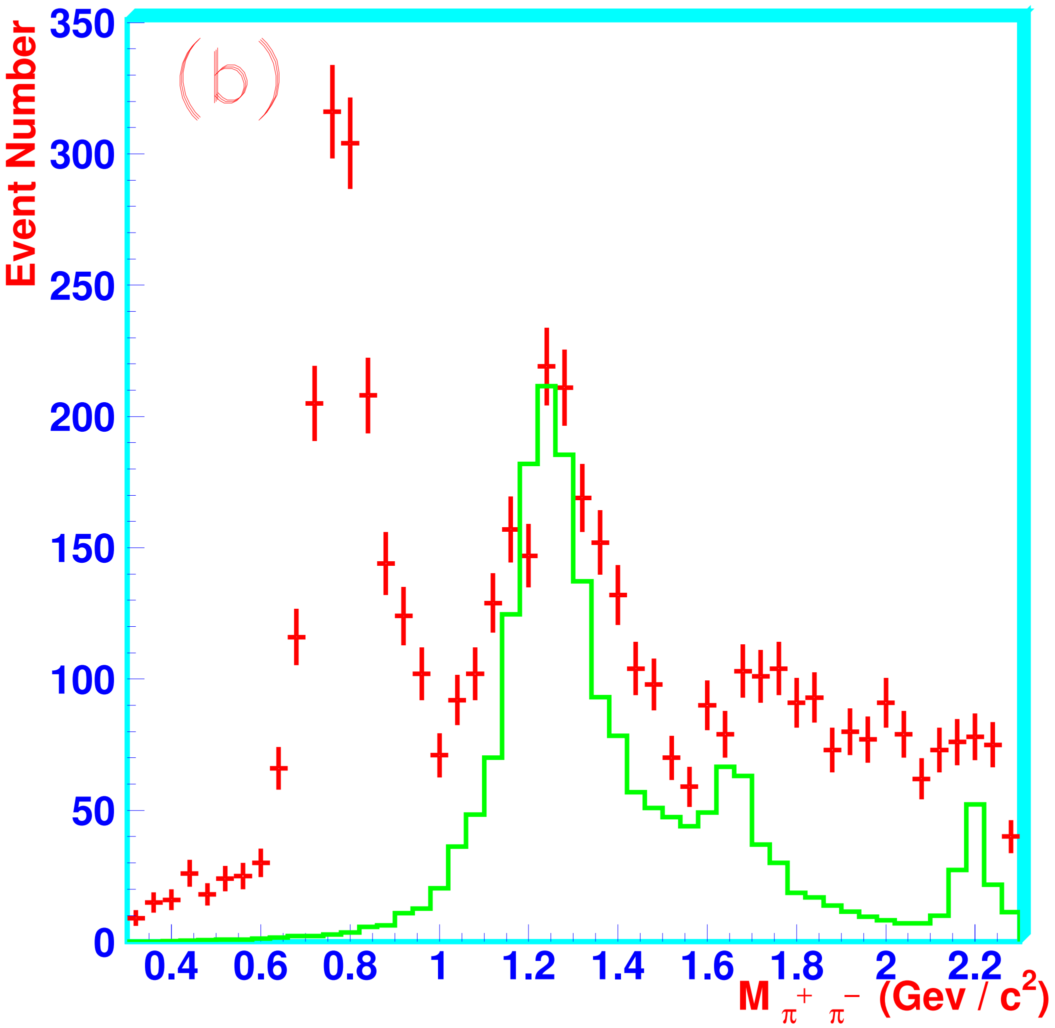

Figure 52: total 2^{++}

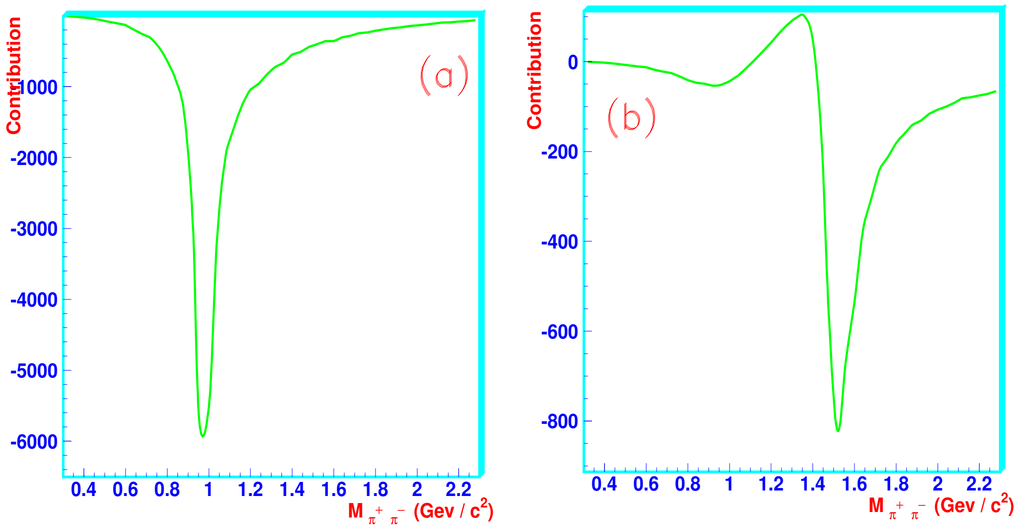

Figure 53: (a) Interference between $f_0(980)$ and $f_0(1030)$ and (b) interference between $f_0(1500)$ and $f_0(1030)$

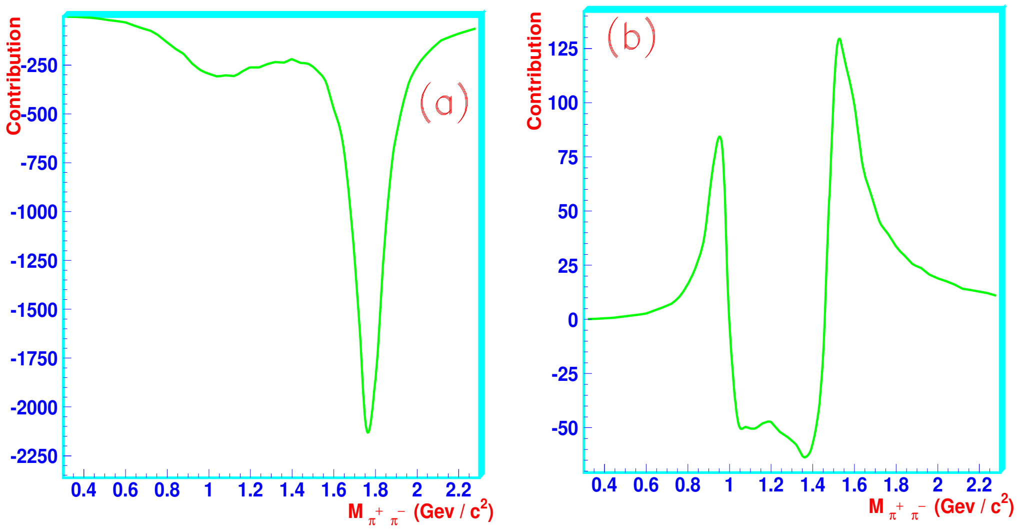

Figure 54: (a) Interference between $f_0(1770)$ and $f_0(1030)$ and (b) interference between $f_0(980)$ and $f_0(1500)$

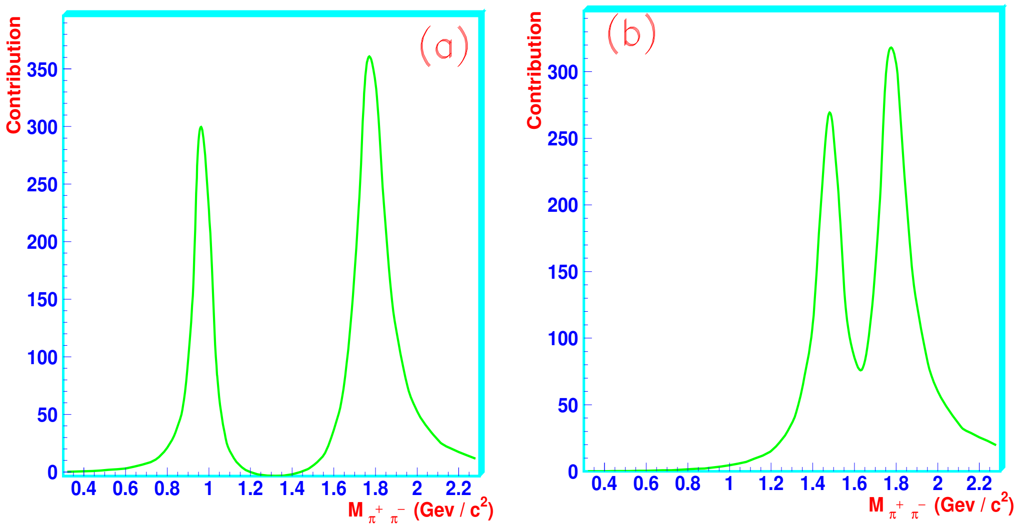

Figure 55: (a) Interference between $f_0(980)$ and $f_0(1770)$ and (b) interference between $f_0(1500)$ and $f_0(1770)$

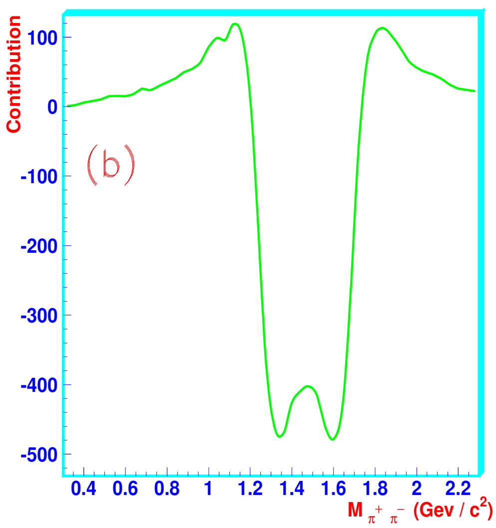

Figure 56: interference between $f_2(1270)$ and $f_2(1710)$

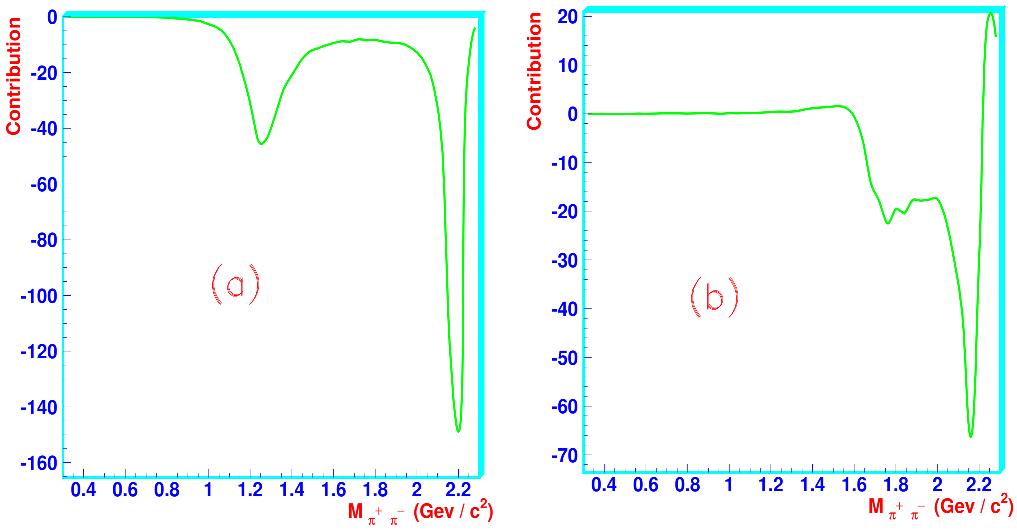

Figure 57: (a) Interference between $f_2(1270)$ and $f_2(2230)$ and (b) interference between $f_2(1710)$ and $f_2(2230)$

resonances	Branch Ratio($\times 10^{-4}$)
$f_2(1270)$	$8.34 \pm 2.49 \pm 0.21$
$f_0(980)$	$3.70 \pm 1.40 \pm 0.14$
$f_0(1500)$	$2.47 \pm 1.03 \pm 0.12$
$f_2(1710)$	$1.21 \pm 0.66 \pm 0.08$
$f_0(1770)$	$2.60 \pm 0.82 \pm 0.12$
$f_4(2050)$	$1.57 \pm 0.49 \pm 0.10$
$f_2(2230)$	$0.305 \pm 0.116 \pm 0.043$
$f_0(1030)$	$11.60 \pm 3.94 \pm 0.25$
$\rho\pi$	$120.0 \pm 48.6 \pm 2.2$
$\rho^0\pi^0$	$41.6 \pm 16.8 \pm 1.0$

Table 7: Branching ratio for various resonances.(The first error is systematic and the second error is statistical.)

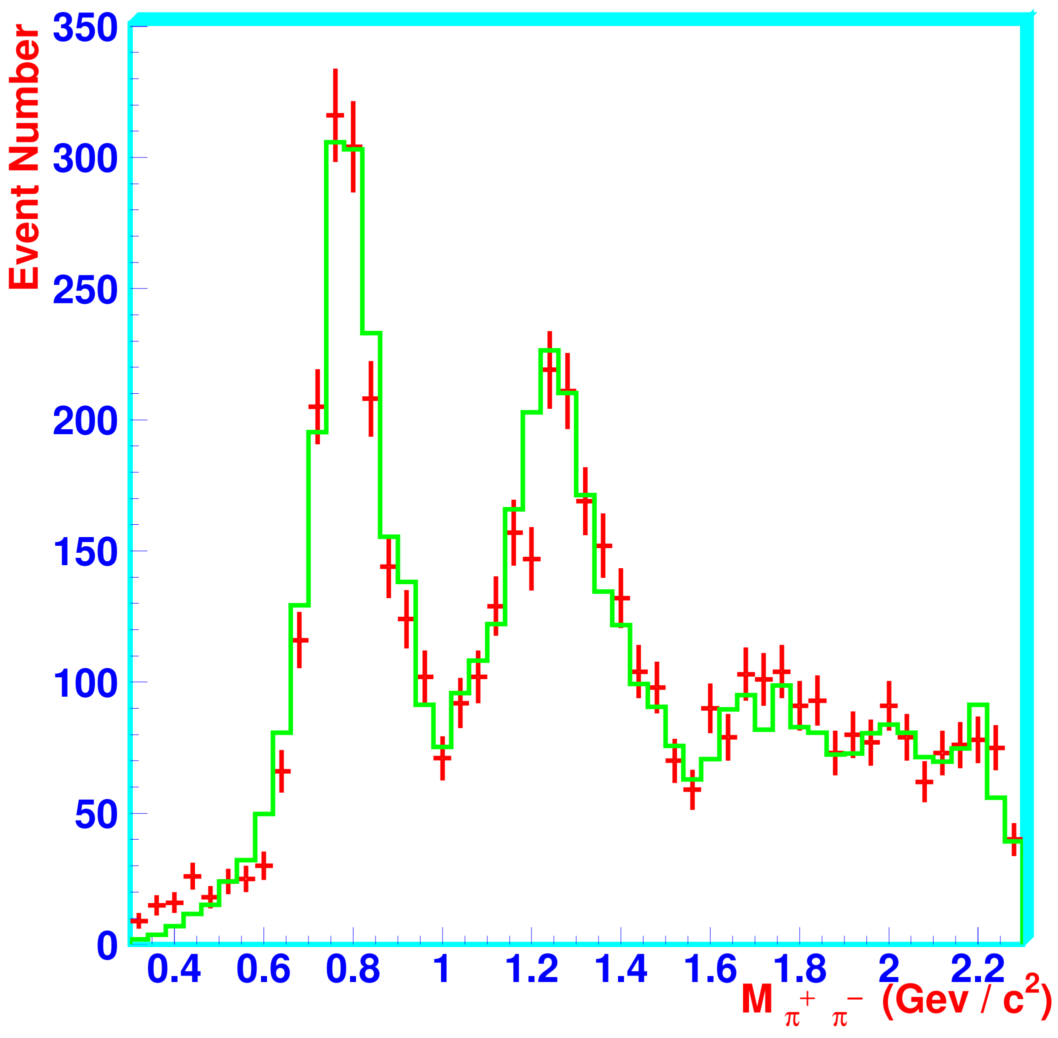

Figure 58: Global Fitting

Acknowledgement: The BES group acknowledges financial support from the Chinese Academy of Sciences and thanks the staff of IHEP for technical support in running the experiment. We also acknowledge financial support from the Royal Society for collaboration between Chinese and UK groups.

References

[1] ? Franklin et al., SLAC-254 (1982).

[2] R.M. Baltrusaitis et al., Phys. Rev. D35 (1987) 2077.

[3] L.P.Chen et al., Nucl. Phys. (Proc. Suppl.) B21 (1991) 80

[4] J.-E. Augustin et al., Z. Phys. C36 (1987) 369.

[5] J.-E. Augustin et al., Phys. Rev. Lett. 60 (1988) 2238.

[6] Particle Data Group, Euro. Phys. J. C3 (1998) 1.

[7] ? Armstrong et al., Phys. Lett. B227 (1989) 186.

[8] W. Dunwoodie, AIP Conf. Proc. ?

[9] D.Barberis et al., Phys.lett. B453 (1999) 305 and 313

[10] BES publication

[11] D.V. Bugg et al., Phys. Lett. B353 (1995) 378.

[12] A. Anisovich et al., Phys. Lett. B419 (1999) 154

[13] A. Abele et al., Nucl. Phys. A609 (1990) 562.

[14] D.V. Bugg, A.V. Sarantsev and B.S. Zou, Nucl. Phys. B471 (1996).

[15] J.Z.Bai et al., Phys. Rev. Lett. 77:3959-3962:1996

[16] J.Z.Bai et al., Phys. Rev. Lett. 76:3502-3505:1996

[17] S.U.Chung, Spin Formalisms (CERN Yellow report, No. CERN 71-8, Geneva, Switzerland, 1971)

[18] S.U.Chung, Phys. Rev. D48(1993) 1225

[19] Ning Wu, Covariant Helicity Analysis of Decay Process

[20] Ning Wu, report on postdoctorial research

[21] BES collaboration, Experimental Study of J/ψ Radiative Decay to K^+K^-

[22] B.Jean-Marie, in:Proc. 23rd Intern. Conf. on High Energy Physics (Berkeley, CA, 1986)

[23] L.Kopke and N.Wermes, J/ψ decays, Phys.Reports, 174, Nos.2-3(1989)67-227